C.N.R.S.
Centre National de la Recherche Scientifique

I.N.F.N.
Instituto Nazionale di Fisica Nucleare

Selection and DC characterization of the control photodiodes for Advanced Virgo

Arnaud Bellétoile

LAPP - IN2P3 - CNRS

9, chemin de Bellevue - 74941 Annecy le Vieux - France

VIR-0478A-10

Issue 1
Date: August 10, 2010

VIRGO * A joint CNRS-INFN Project
Project office: Traversa H di via Macerata - I-56021 S. Stefano a Macerata, Cascina (PI)
Secretariat: Telephone (39) 50 752 521 – Fax (39) 50 752 550 – e-mail virgo@pisa.infn.it

Contents

Abstract

In order to answer requirements settled by the Advanced Virgo (AdV) design, the detection system has to be redrawn. This note focuses on the DC measurement made on the photodiodes to be used in the control system. Basic requirements are reminded, selection process and DC characteristics are presented. Conclusive statement should arise from a foreseen note that will take account for AC measurements as well.

Feature	Quant. Eff.	C_s	R_s	I_{dark}	Diam.	I_{ph}
typ. Value	95 %	280 pF*	10 Ω*	10 nA*	3 mm	100 mA

Table 1: Typical values of features from the former Virgo InGaAs photodiodes manufactured by Hamamatsu. The * mark stands for values under a bias voltage $V_b = 10$ V.

1 Basic requirements

The initial Virgo detection photodiodes were InGaAs PIN devices manufactured by Hamamatsu and exhibit performances that are still, more than 15 years later, very difficult to reach. Unfortunately those components are not available anymore making a new design of the detection readout a necessity due to long term maintenance considerations. Furthermore, the modulation frequencies foreseen on AdV settles additionnal constraints on the photodiode in terms of bandwidth. Indeed, it is foreseen that AdV uses a triple phase modulated beam with the highest modulation frequency in the range of $50 - 80$ MHz. Moreover, it should be possible to access the signal at twice this frequency, which means a detection system that could handle frequency as high as 160 MHz or so. This is well above the initial Virgo detection system capabilities.

Due to alignement facility and limited beam size reduction (in order to reduce back scattered light), the effective area of the photodetector should remain approximately the same as for the previous one, that is to say a diameter of 3 mm. This characteristic is in defavour of a wide frequency bandwidth as a photodiode bandwidth scales inversely with its stray capacitance which is proportionnal to its effective area.

Another point lays in the fact that some of the detection port impose photodiodes to be placed under vacuum. This impacts on the power dissipation of the system on the one side, and on the ability of the photodiode to handle high intensity beam on the other side. The latter item can be converted into a reduction of the number of photodiodes on a given port and, consequently, into a reduction of the effective load. It appears that an incident optical power of 100 mW, the same as required for Virgo, would be sufficient as a starting point.

Finally, the detection system should offer at least the same, or improved, quality response in terms of high quantum efficiency, high linearity and low noise features as the previous one used on Virgo. On a practical aspect, it appears that 15 years of technical developpement offer rather poor improvement, if not regression, on the photodiodes characteristics in the wavelength range of interest. So that redoing the same as 15 years earlier allready reveals as a challenging task.

The main Virgo photodiode characteristics are summarized in table 1 as a guide for the new selection.

2 Choice of the set of components

It should be first stated that our attention was directed toward InGaAs detector. Despite the disadvantages that could suffer an alloy like InGaAs in terms of high power handling and linearity compared to a pure material such as Ge photodetectors, the gain offered by its highest efficiency at $\lambda = 1.064\,\mu$m makes it, from far, the most promising material.

From an exhaustive review of available commercial photodiodes, we first retained 7 manufacturers of large area (diam. 3 mm) InGaAs PIN photodetectors listed in table 2. Among those 7 manufacturers, we purchased components from only 3: Perkin Elmer, Fermionics and Judson. Other devices beeing eliminated because they did not fulfill one or more of the mandatory criterion listed below:

- a maximum photocurrent of, at least, 100 mA in order to handle a sufficiently high optical power and avoid damages,
- a quantum efficiency higher than 80 % without anti-reflection coating for SNR considerations,
- a stray capacitance lower than 400 pF together with a maximum bias voltage higher than 10 V to ensure both a large frequency bandwidth and a wide dynamic,
- a dark current lower than some 10 nA in order to minimize additive noise.

Manufacturer - Reference	Purch.	Reason
Hamamatsu - G8376-SPL	No	$I_{ph} \leq 10\,\text{mA}$, $C \sim 500\,\text{pF}$*
eGTran - PD3M-001	No	$I_{ph} \leq 20\,\text{mA}$, $V_b < 2\,\text{V}$, $I_{dark} \leq 50\,\text{nA}$
Perkin Elmer - C30664	Yes	-
Roithner Laser. - PT811	No	$I_{ph} \leq 10\,\text{mA}$, $C \sim 800\,\text{pF}$*, $I_{dark} \leq 200\,\text{nA}$
Fermionics - FD3000W	Yes	-
GPD Opto. - GAP3010	No	$I_{ph} \leq 10\,\text{mA}$
Judson - J22-8I-HP	Yes	-

Table 2: List of large area InGaAs PIN photodiode manufacturers and reference of the device of interest, status (purchased or not) and reason if not purchased. I_{ph} stands for maximum photocurrent, V_b for maximum bias voltage, I_{dark} for dark current and C for capacitance. The * mark means that the value is obtained with a 10 V bias voltage applied on the photodiode.

The judson photodiode is a recent development of back-illuminated photodiode whereas to 2 others are usual front illuminated components. This should offer a higher linearity, due to lower fluctuations in the value of the serial resistance, and better tolerance to high optical power. Several photodiodes of each type were purchased in order to check for reproducibility of the measurements. Due to cost considerations and availability of the devices, we get 3 from Fermionic, 5 from Perkin Elmer and 2 from Judson.

A couple of remarks about manufacturers should be addressed. First, Hamamatsu who provided the initial set of Virgo photodiodes can not guaranty as good requirements as 15 years ago. After discussions with people from Hamamatsu, it appeared that only a specific selection of components could guaranty similar (but still below) performances with a cost per unit increased by one order of magnitude. Then, eGTran photodiodes were selected for the Advanced LIGO experiment. From our point of view, those devices present rather poor performances and so were not retained.

Beside commercial solution, we joined some discussion initiated by the Nice group with a french laboratory of the CNRS, the CHREA, working in the field of semiconductor material to investigate more specialized components. Unfortunately, a specific component would have required a full design that wouldn't have been compatible with both, our time scale and budget.

3 DC measurements

3.1 Dark current

The first measurement performed was the dark current I_{dark} on each photodiode. This is a residual current flowing whereas no light is impinging the sensitive area. It constitues an additive noise and reflects somehow the quality of the semiconductor. We are expected as low value of I_{dark} as possible. Typical value of I_{dark} beeing in the range of 1 nA or so, its measurement is quite tricky and implies the use of dedicated Pico-Ammeter together with a proper shielding to avoid parasitics. The measurement setup uses a Keithley 487 pico ammeter with a 10 fA sensitivity.

Results are summarized on a log scale on figure 1 and on a linear one for the best devices on figure 2. The Perkin Elmer photodiodes exhibit both the best and the worst results. It seems that 2 of the 5 components come from a bad batch. One of those faulty devices is above datasheet specifications and will be replaced by the manufacturer, the other one lies just below. This illustrates the scattering from one batch to the other and the need of several devices to get an average idea of their performances. Other photodiodes exhibit good values of dark current, well below 10 nA.

3.2 Equivalent electrical scheme

From an electric point of view, PIN photodiodes such as those we are using can be expressed as an equivalent electrical scheme depicted on figure 3. The capacitance C_s is called the junction Capacitance. It originates from the presence of an equal amount of p and n charges on each side of the intrinsic high resistivity layer (the so called "I" layer). Associated to the ohmic losses induced resistance R_s, this parameter limits the usable bandwidth by providing the device a R-C tranfert function of the form given in eq. 1.

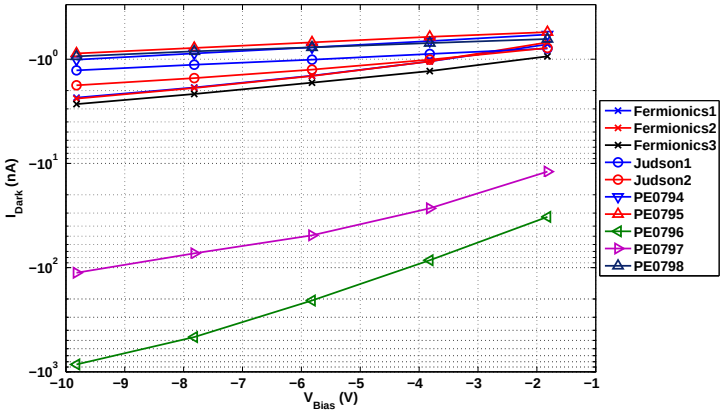

Figure 1: I_{dark} measurement results for each photodiode (legend on the figure) as a function of the bias voltage. The y-scale is logarithmic so all devices appears on the plot. Please note that dark currents values are negative due to convention considerations.

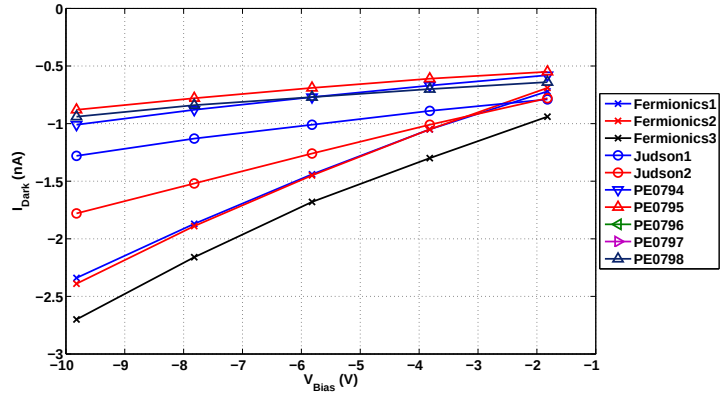

Figure 2: Subest of I_{dark} measurement results for each photodiode (legend on the figure) as a function of the bias voltage on a linear scale. The devices labelled PE0796 and PE0797 do not appear on this plot because their dark current is out of scale.Please note that dark currents values are negative due to convention considerations.

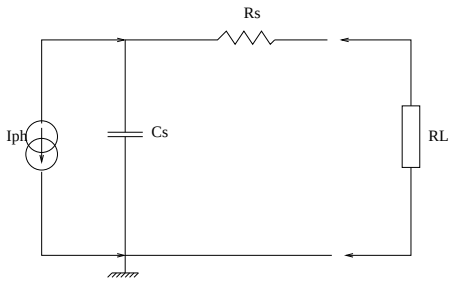

Figure 3: PIN photodiode equivalent electrical scheme loaded by an R_L impedance.

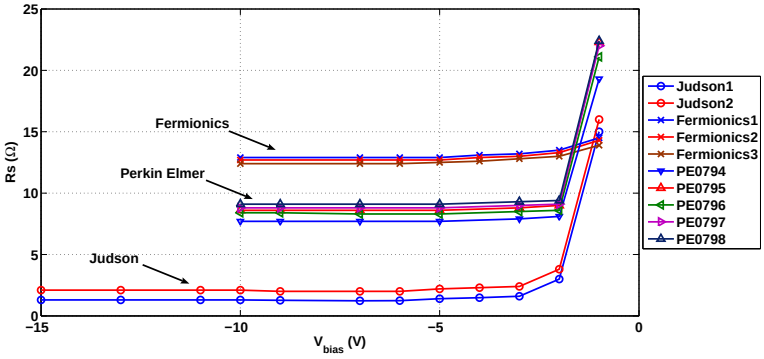

Figure 4: Serial resistance R_s in Ω for each photodiode as a function of the applied bias voltage. Measurements were made using a HP 4284 CLR-meter at 1 MHz.

$$V_s = \frac{R_L}{\sqrt{1 + \left(\frac{\omega}{\omega_c}\right)^2}} \times I_{ph} \tag{1}$$

with $\omega_c = \frac{1}{(R_s+R_L)\times C_s}$, I_{ph} the photodiode photocurrent, V_s the device output voltage, R_s and C_s the device electrical characteristic and R_L the load resistance.

As mentionned above, the C_s value scales linearly with the effective area of the component and with the inverse of the thickness of its I layer. Whereas the effective area has to remain constant for pratical purposes, the I thickness can be increased by applying a bias voltage on the component so that the C_s value is reduced by an equal amount.

Both R_s ans C_s parameters were determined for each photodiode using a CLR-meter (ref. HP 4284A) at a frequency of 1 MHz. The electric model used to interpret the reflectivity measurements is made up of a serial capacity and resistance so that they can be directly identified to those on figure 3. Indeed the current source is, first, an open circuit with no incident light and, then, appears in parallele to C_s with incident light because flowing charges orginate from the junction, accross the I layer.

Results are presented on figure 4 for the serial resistance and on figure 5 for the serial capacitance. Characteristics offer a good reproducibility from one component to the other. As expected, the Judson photodiodes exhibit both the lowest capacitance and resistance values making them the most promising device in term of frequency bandwidth. It should also be noted that a bias voltage of -10 V is sufficient as no significant improvement of C_s appears with higher values.

3.3 Linearity and quantum efficiency

The next parameter to be determined is the DC linearity as a function of the incident optical power. This allows us to extract estimations for both the quantum efficiency and the linearity of the devices. The

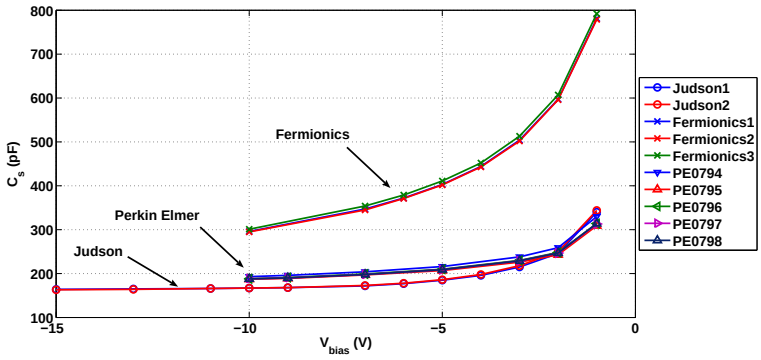

Figure 5: Serial capacitance C_s in pF for each photodiode as a function of the applied bias voltage. Measurements were made using a HP 4284 CLR-meter at 1 MHz.

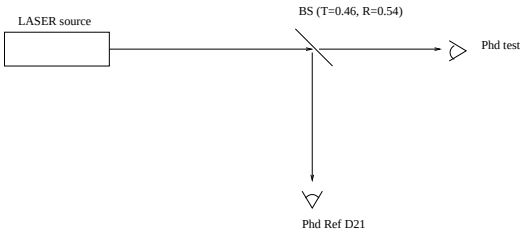

Figure 6: DC linearity measurement setup.

first one beeing estimated from the slope of the adjusted response of the photodiode, the second from the dispersion from this model.

For this measurement, we had to face the difficulty of finding an absolute estimation of the optical power of the laser beam. Devices like optical power meters offer an accuracy of approximately 10 % which is too large for our concern. Instead, we used one of the previous Virgo photodiodes as a reference to our measurement. This photodiode is labelled "D21" and, from previous estimations (years ago...), exhibits a quantum efficiency of 97 %. Whatever the accuracy of this number is, our measurements reflect a trusted relative estimation of the new set of photodiodes capabilities.

The measurement setup is depicted on figure 6. The optical power of the beam is modified directly on the source front panel. The beam is splitted on a beam splitter of $T = 0.46$ & $R = 0.54$, which values have been measured within 1 %, and signals, from both the photodiode under test and the D21 photodiode, are digitized using Virgo amplifier, demodulation board and ADC. The overall DC transimpedance gain of the acquisition channel has been measured as:

$$V_{out}(\mathrm{V}) = 0.109 \times I_{in}(\mathrm{mA}) \tag{2}$$

For each data set, the optical power of the beam is slowly increased from zero up to a maximum value, then decreased back to zero again. The maximum value is given by the dynamic of the electronic which is close to 90 mW (corresponding to an output voltage of 8 V). On each data set, a simple linear model was fitted. The slope reflects the relative quantum efficiency of a given photodiode with respect to the D21 reference photodiode as illustrated on figure 7.

The estimation of linearity is somehow tricky as it should take account for several effects like saturation, dispersion, thermal effect due to the incident power, etc. ... We therefore estimate linearity using the residual of the above linear fit. As the residual distribution is not a gaussian one (and is not expected to be), we rather use the width of the residual distribution as illustrated on figure 8.

As our most important source of error is due to miss-alignement of the photodiodes, those measurements were repeated 5 times for each photodiode (with a complete replacement of the component...) to get an most accurate estimation of the parameters. The final results for each photodiode are summarized in table 3 for both the quantum efficiency and the linearity. It appears that Fermionics photodiodes

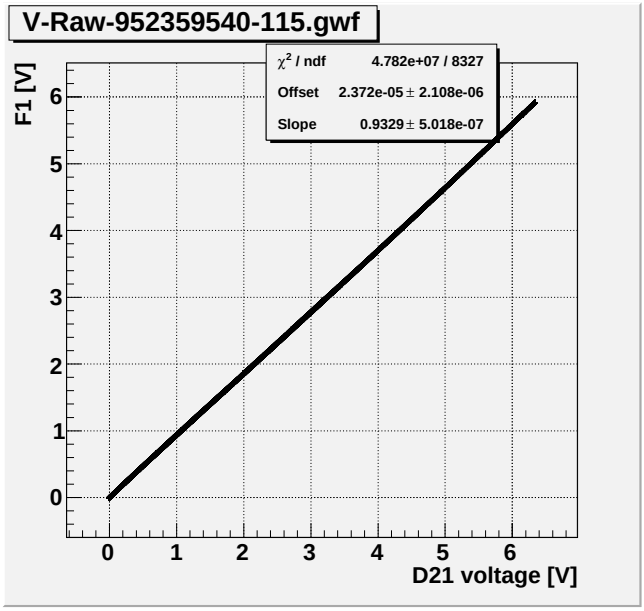

Figure 7: Linear fit of the measured output voltage in V. The reference photodiode, D21, is on the X-axis and the device under test, here Fermionics 1, on the Y one. Systematics are corrected so the adjusted parameters on the plot reflects the true relation between quantum efficiency of the 2 photodiodes.

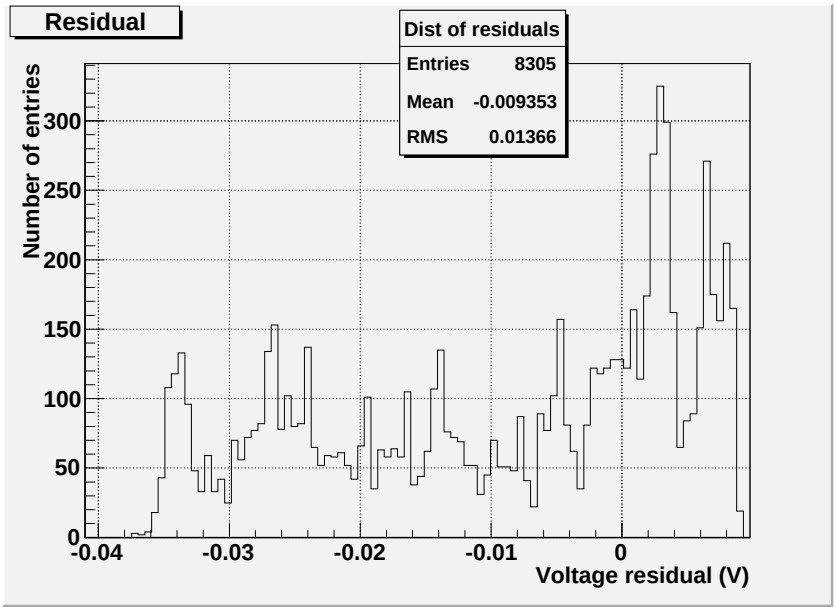

Figure 8: Distribution of residuals from the function adjusted on figure 7. The linearity criterion is defined as the width of this distribution, in this particular example, $lin = 47.6\,\mathrm{mV}$.

Phd	F1	F2	F3	J1	J2
η	$90.5 \pm 1.8\,\%$	$89.6 \pm 2.8\,\%$	$91.1 \pm 2.0\,\%$	$80.2 \pm 0.5\,\%$	$78.1 \pm 1.4\,\%$
linearity	$97.7 \pm 82.7\,\mathrm{mV}$	$55.8 \pm 32.5\,\mathrm{mV}$	$61.0 \pm 32.4\,\mathrm{mV}$	$30.5 \pm 19.0\,\mathrm{mV}$	$35.2 \pm 22.0\,\mathrm{mV}$

Phd	PE94	PE95	PE96	PE97	PE98
η	$87.0 \pm 1.2\,\%$	$87.2 \pm 1.7\,\%$	$87.8 \pm 1.0\,\%$	$88.8 \pm 0.7\,\%$	$88.3 \pm 0.5\,\%$
linearity	$35.6 \pm 13.8\,\mathrm{mV}$	$40.0 \pm 22.0\,\mathrm{mV}$	$33.5 \pm 7.0\,\mathrm{mV}$	$30.8 \pm 7.0\,\mathrm{mV}$	$32.3 \pm 9.4\,\mathrm{mV}$

Table 3: Summarized measured values of the quantum efficiency and linearity for each photodiode. The error bar is determnied by the standard deviation over 5 measurements. For the quantum efficiency, a virgo photodiode with a quantum efficiency of 97 % was used as a reference. Plots from which those values are extracted are joined in the Annex of this note.

	$<\eta>$	$<lin.>$	$<C_s>$	$<R_s>$	$<I_{dark}>$
Fermionics	90 %	72 mV	300 pF	13 Ω	−2.5 nA
Perkin Elmer	88 %	34 mV	190 pF	8 Ω	−1.0 nA∗
Judson	80 %	33 mV	170 pF	2 Ω	−1.5 nA

Table 4: Summarized DC characteristics of the photodiodes for each manufacturer. The mark $*$ refers to a value of I_{dark} without the 2 faulty Perkin Elmer photodiodes.

surprisingly exhibit the best quantum efficiency, followed by the Perkin Elmer components. However, those Fermionics suffer a poor linearity which is a factor of 2 above other devices.

Two issues might be mentionned here. First, the measured quantum efficiency for new photodiodes is expected to be lower than the one from Virgo photodiodes as there is no AR coating on the tested devices. This coating implies an important extra cost per unit that will only be justified and paid off for the final purchase. The commonly admitted gain of AR coating is roughly 4 % per interface (so a gain of 8 % per photodiode).

The other point concerns the linearity. Indeed the criterion we used is biased by the linearity of the reference photodiode. Both errors sums quadratically. This is of a minor importance if the photodiode, such as a Fermionics, has a poor linearity compared to the reference but does not allow us to distinguish between the Perkin Elmer and Judson components. We therefore redo the above measurement using a Judson photodiode as a reference but did not see significant improvement.

4 Conclusion

We presented here the photodiode DC characterization. The measurement bench has been defined in order to characterize the set of component to be purchased for the detection system. The DC measurement results are summarized in table 4. It seems that both Perkin Elmer and Judson photodiodes are the most favoured candidate. Indeed, despite their high quantum efficiency, the Fermionics components couldn't offer a sufficient bandwidth. Additionnal AC measurements are needed to bring a conclusive statement. A prerequisite of those AC measurements is the design of suitable preamplifier, which, in turn, implies the knowledge of the device to be used with it. Those issues will be discussed in a forecoming note.

A Fermionics 1

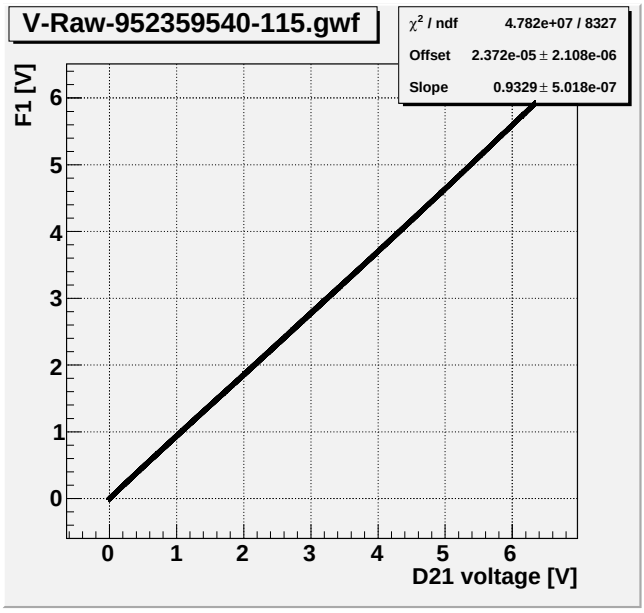

Figure 9: Linear fit #1 of Fermionics 1

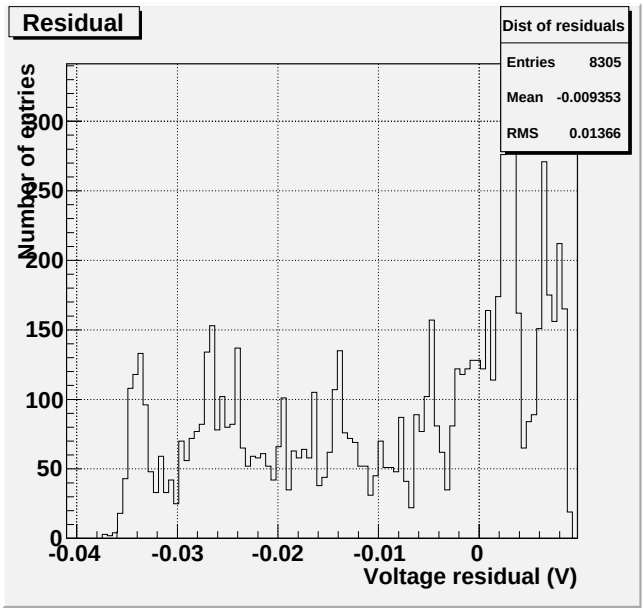

Figure 10: Residual distribution #1 of Fermionics 1

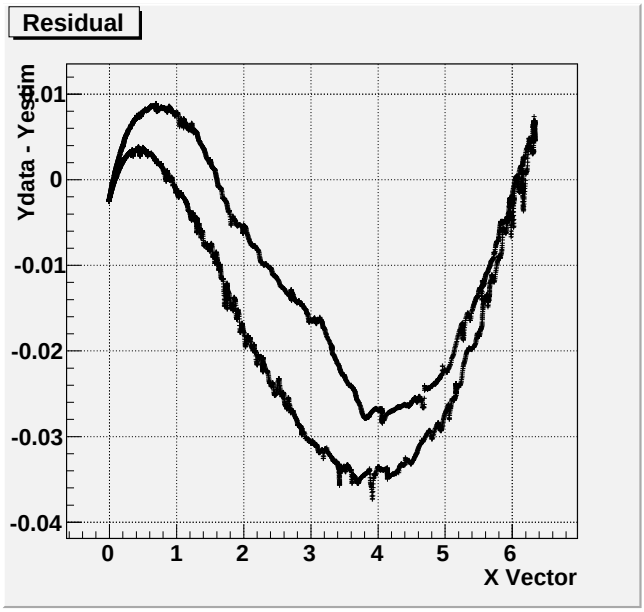

Figure 11: Residual plot #1 of Fermionics 1

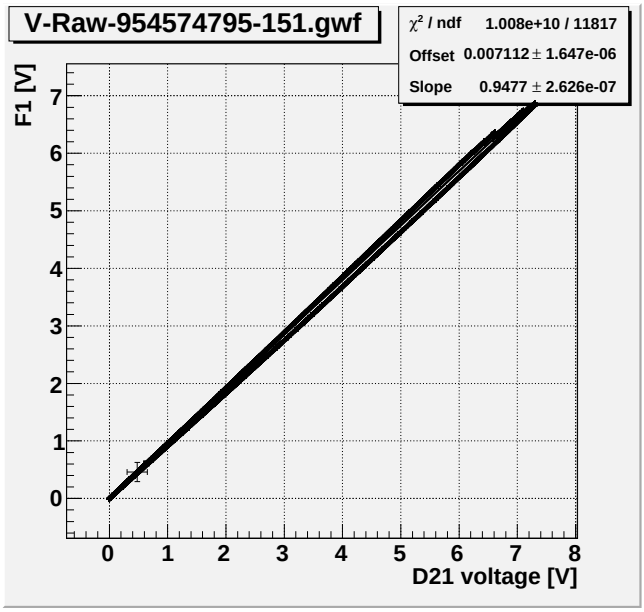

Figure 12: Linear fit #2 of Fermionics 1

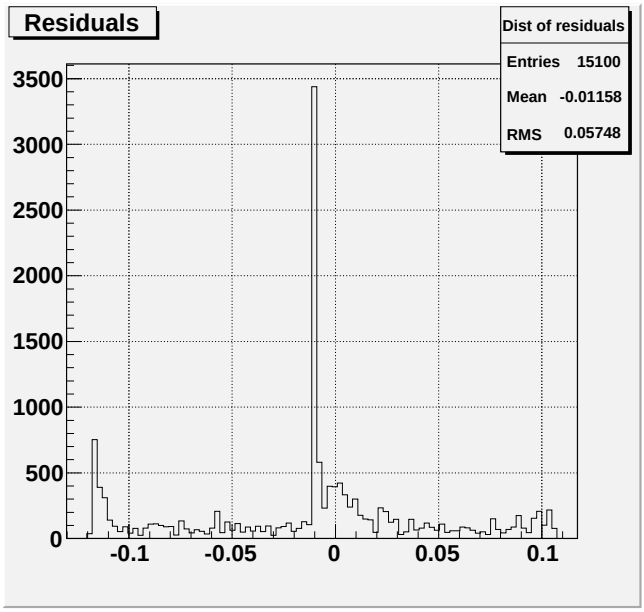

Figure 13: Residual distribution #2 of Fermionics 1

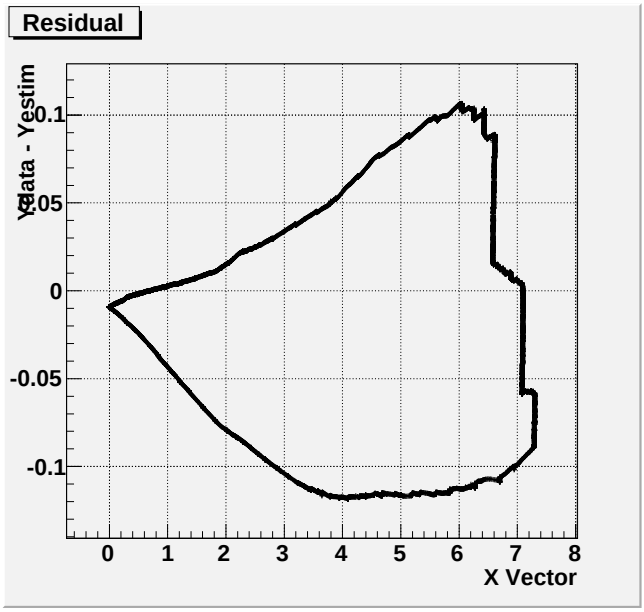

Figure 14: Residual plot #2 of Fermionics 1

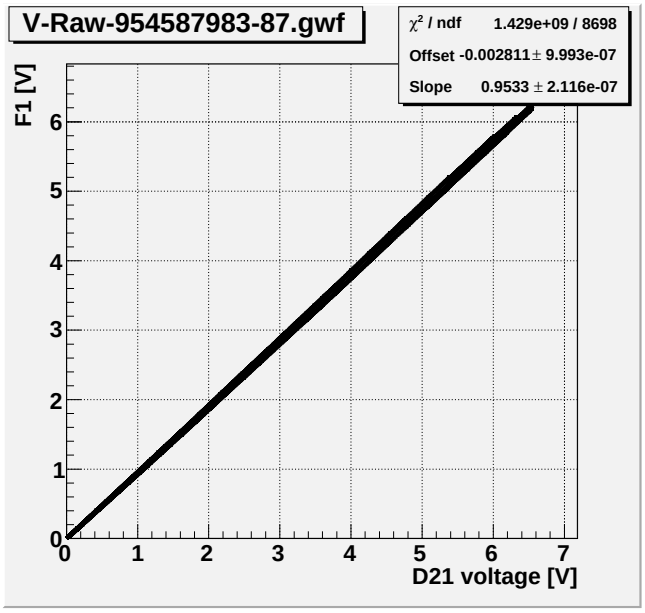

Figure 15: Linear fit #3 of Fermionics 1

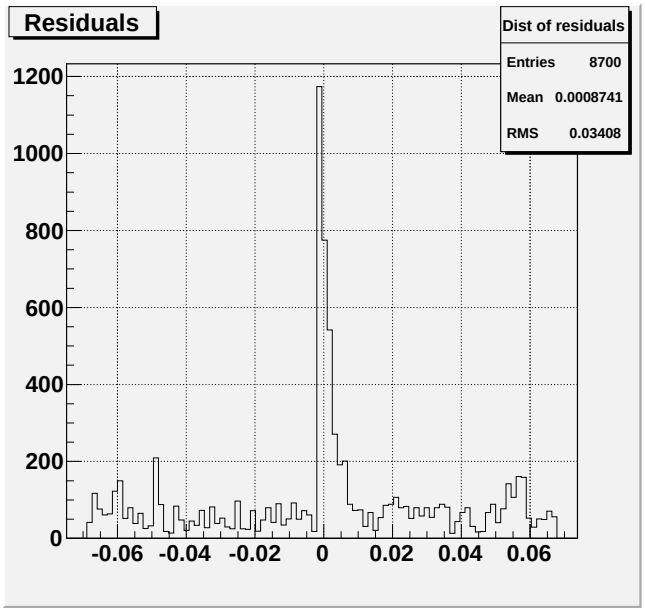

Figure 16: Residual distribution #3 of Fermionics 1

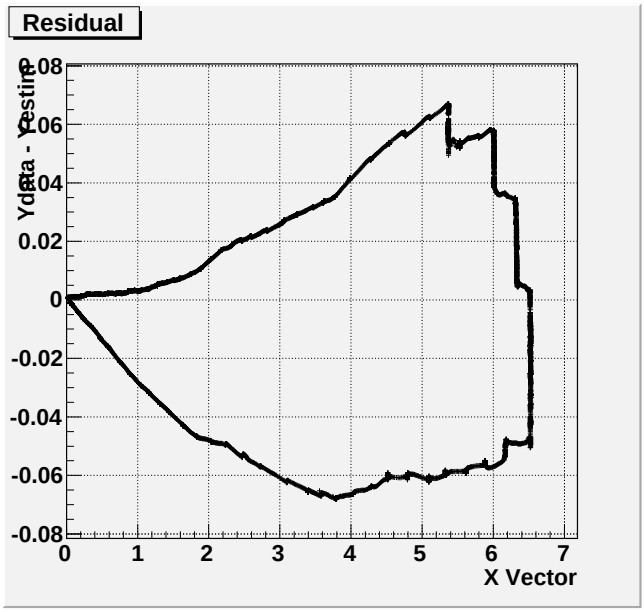

Figure 17: Residual plot #3 of Fermionics 1

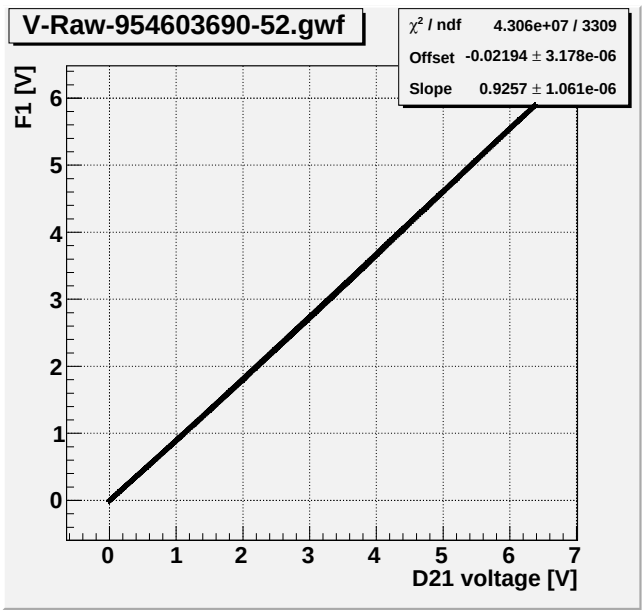

Figure 18: Linear fit #4 of Fermionics 1

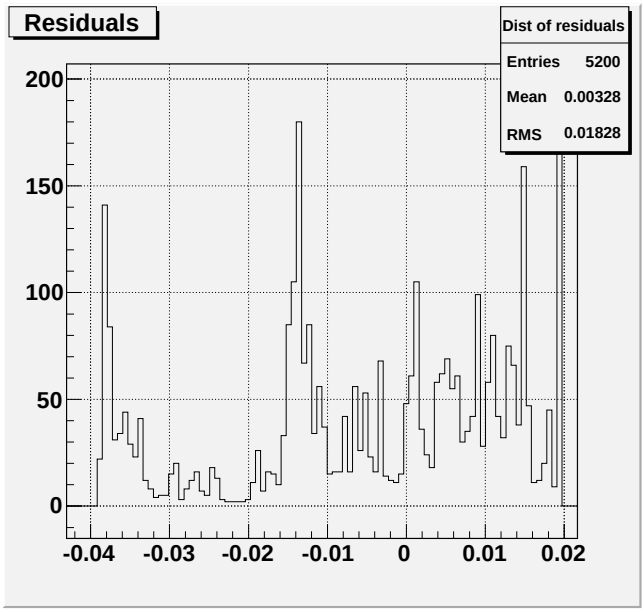

Figure 19: Residual distribution #4 of Fermionics 1

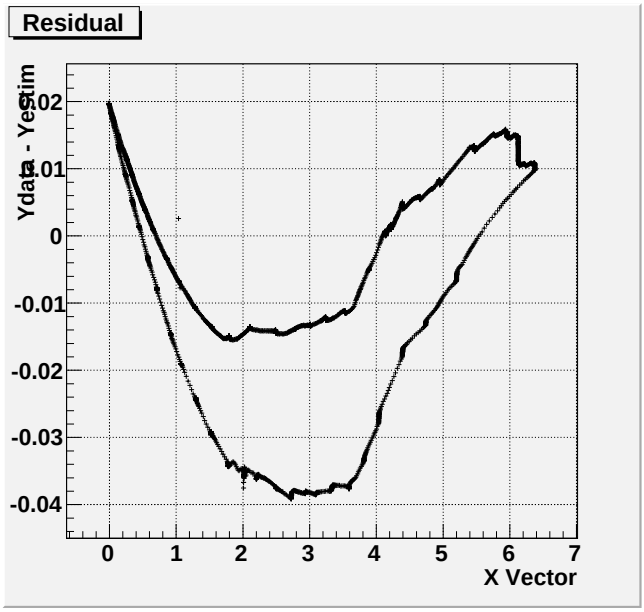

Figure 20: Residual plot #4 of Fermionics 1

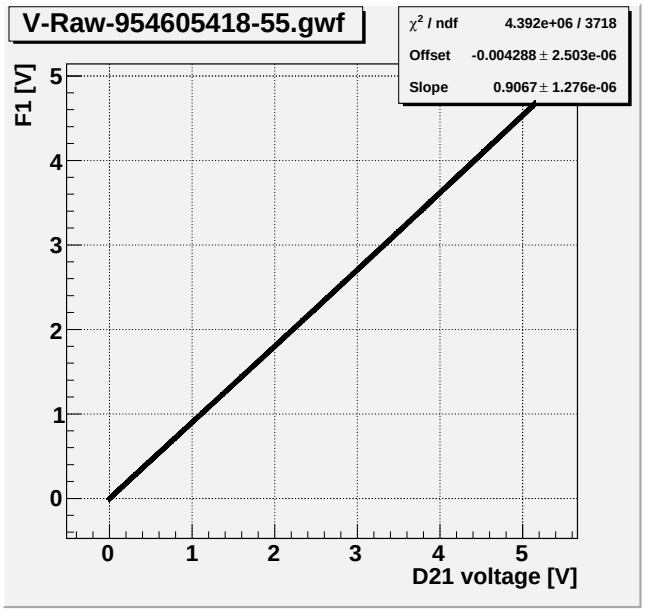

Figure 21: Linear fit #5 of Fermionics 1

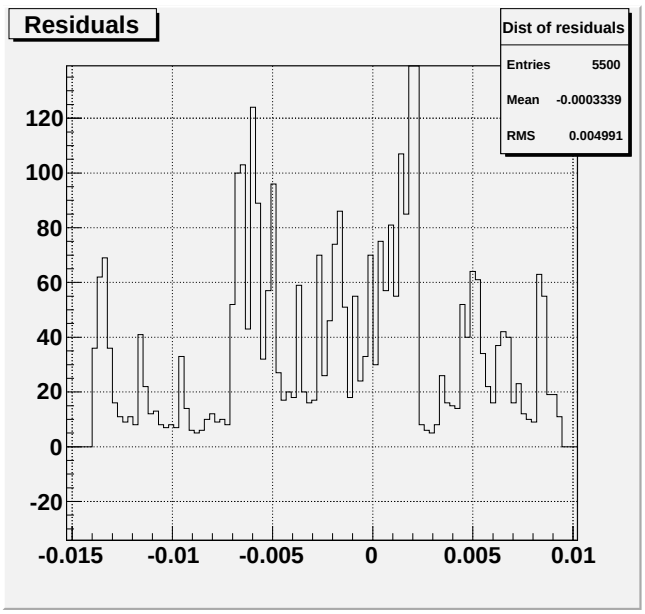

Figure 22: Residual distribution #5 of Fermionics 1

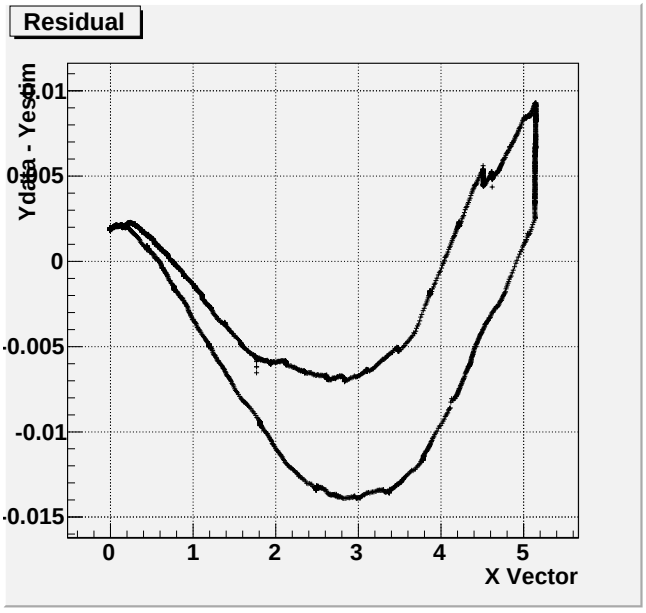

Figure 23: Residual plot #5 of Fermionics 1

B Fermionics 2

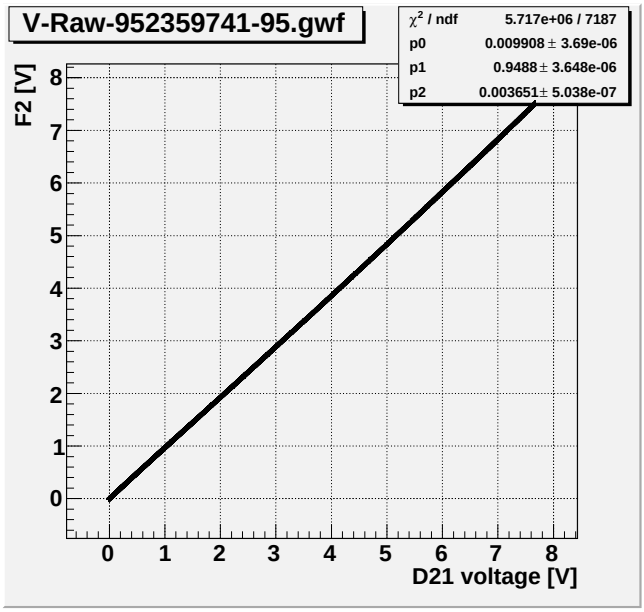

Figure 24: Linear fit #1 of Fermionics 2

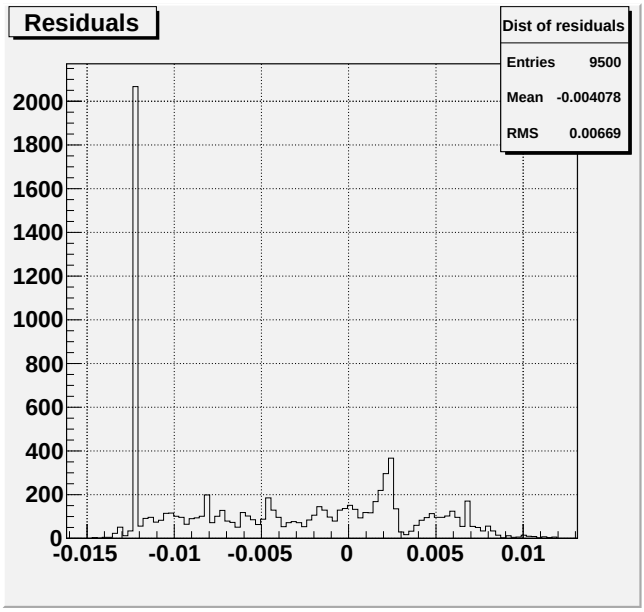

Figure 25: Residual distribution #1 of Fermionics 2

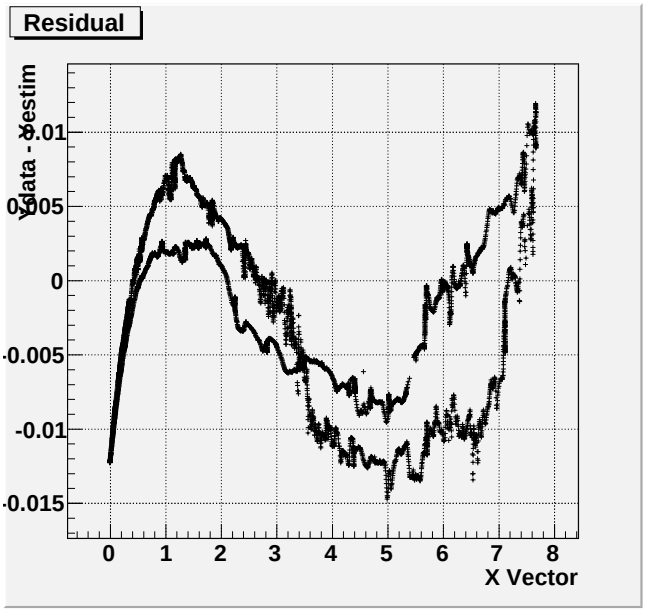

Figure 26: Residual plot #1 of Fermionics 2

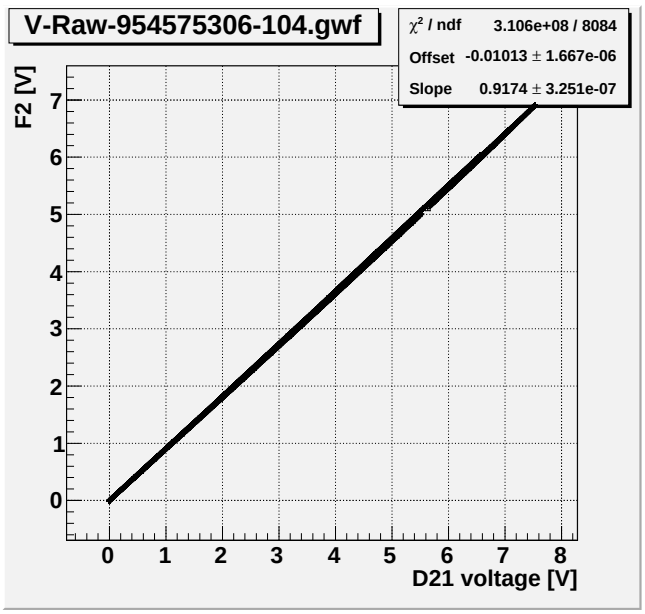

Figure 27: Linear fit #2 of Fermionics 2

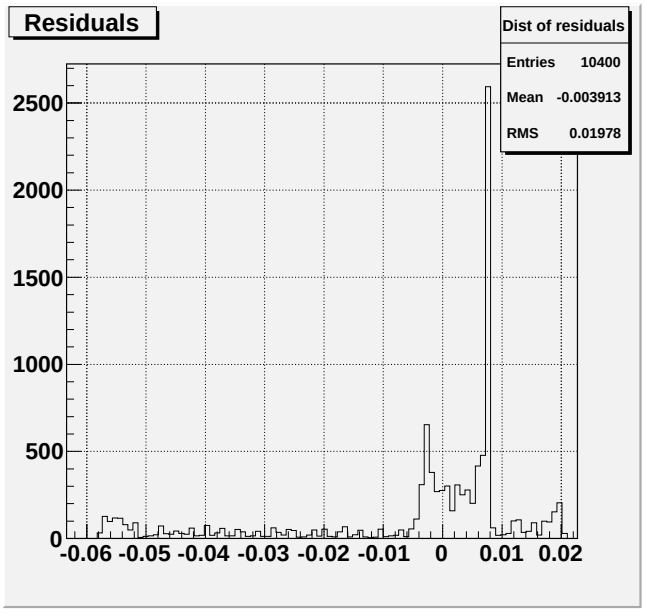

Figure 28: Residual distribution #2 of Fermionics 2

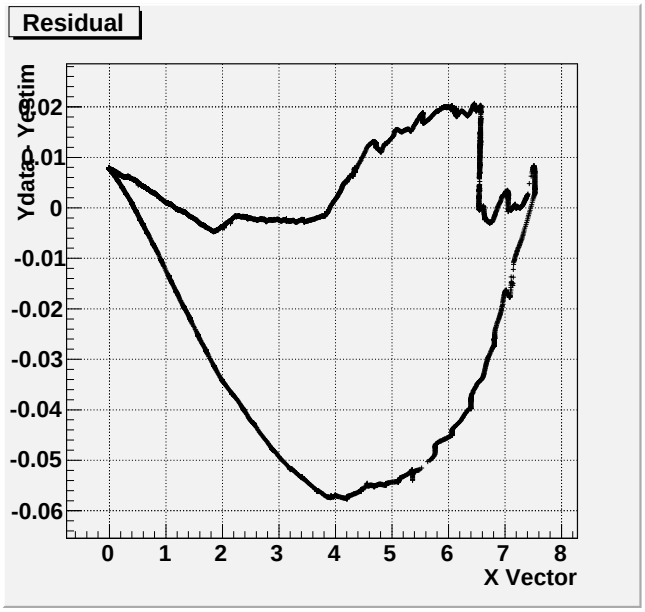

Figure 29: Residual plot #2 of Fermionics 2

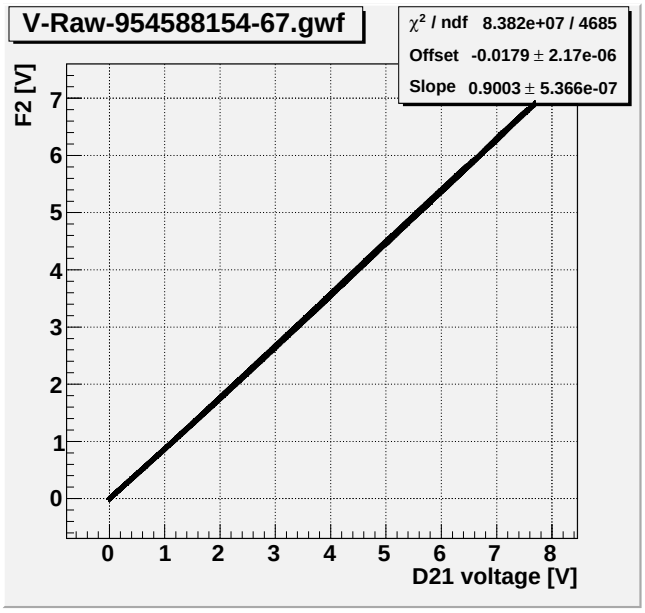

Figure 30: Linear fit #3 of Fermionics 2

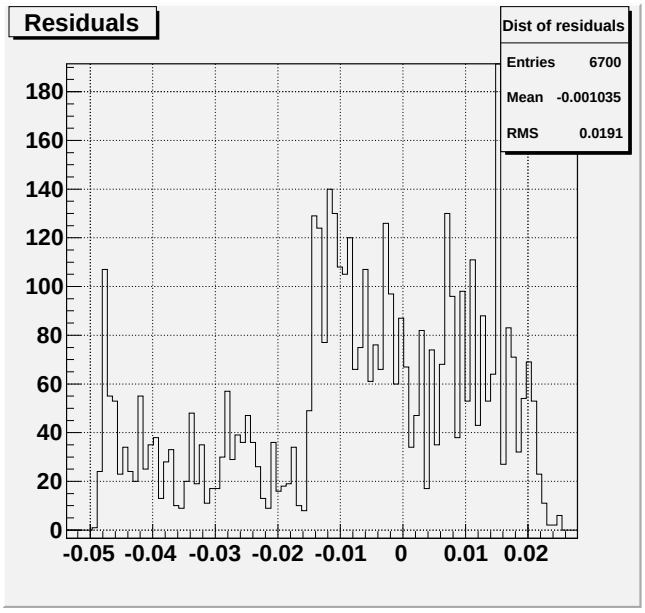

Figure 31: Residual distribution #3 of Fermionics 2

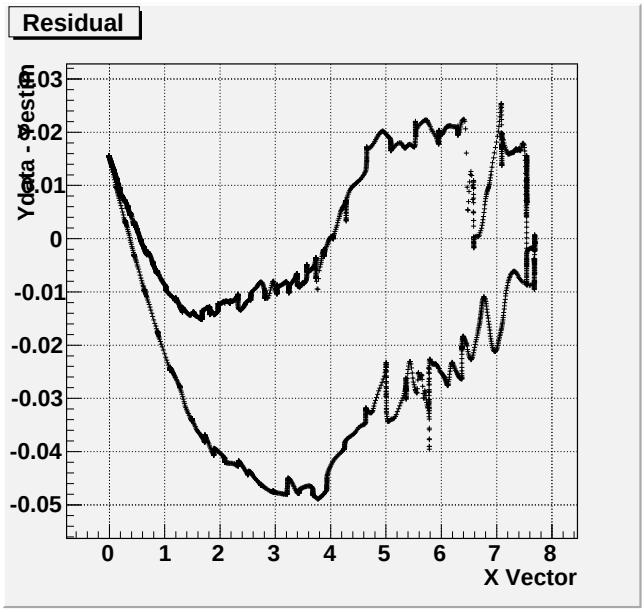

Figure 32: Residual plot #3 of Fermionics 2

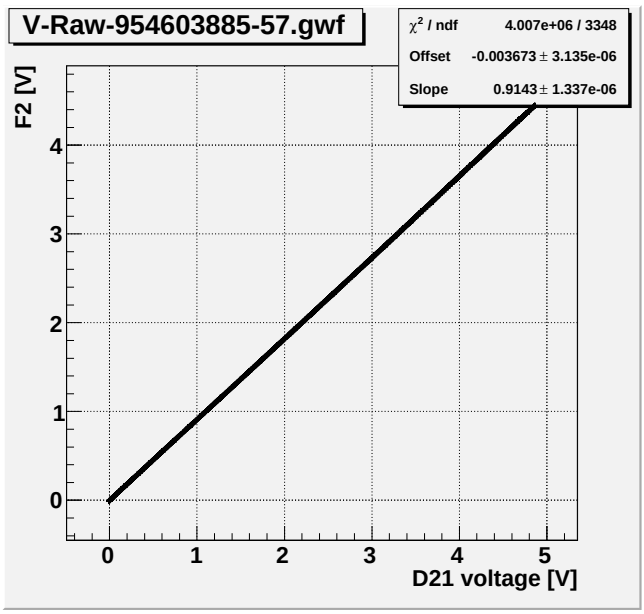

Figure 33: Linear fit #4 of Fermionics 2

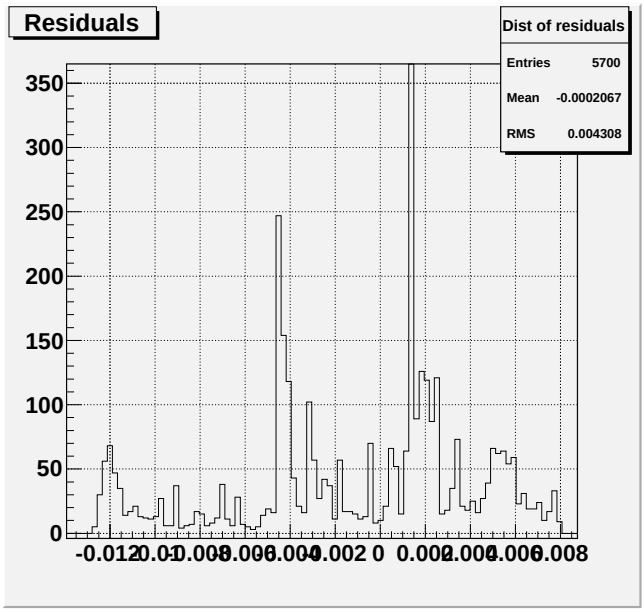

Figure 34: Residual distribution #4 of Fermionics 2

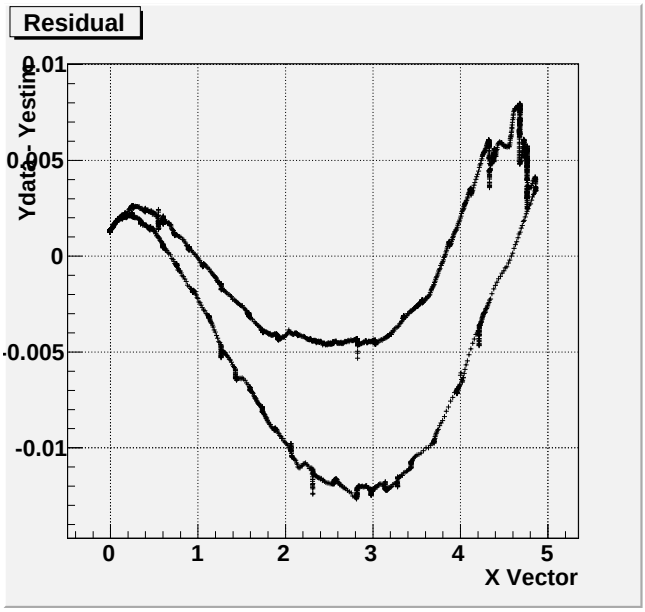

Figure 35: Residual plot #4 of Fermionics 2

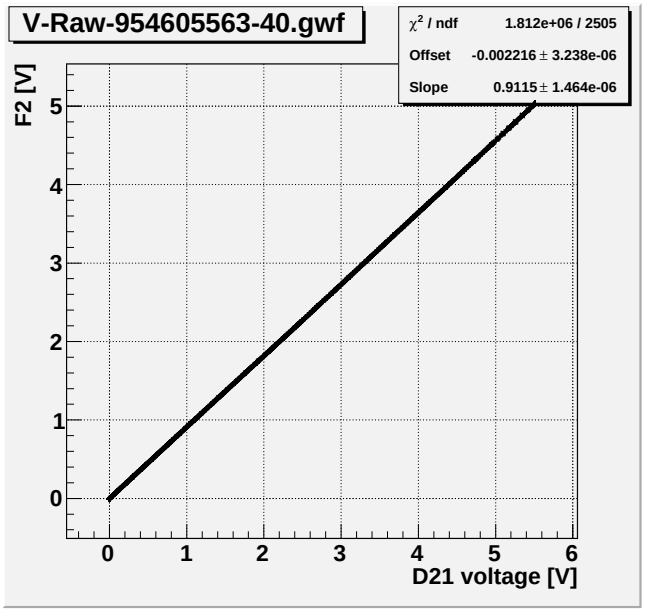

Figure 36: Linear fit #5 of Fermionics 2

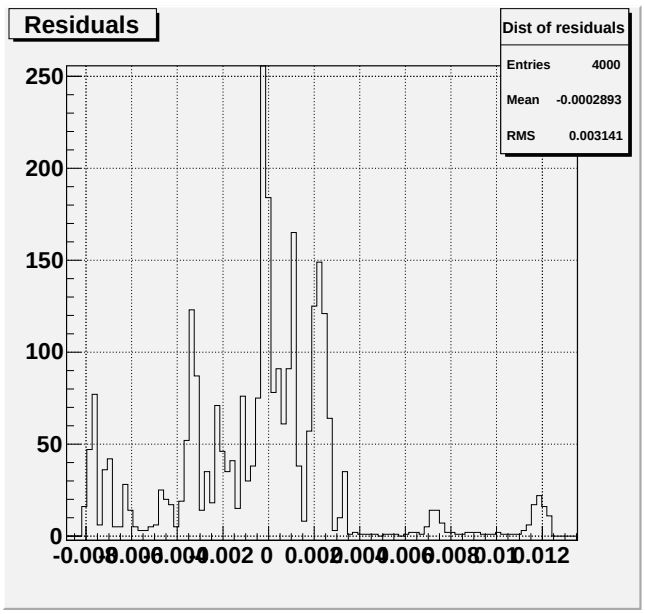

Figure 37: Residual distribution #5 of Fermionics 2

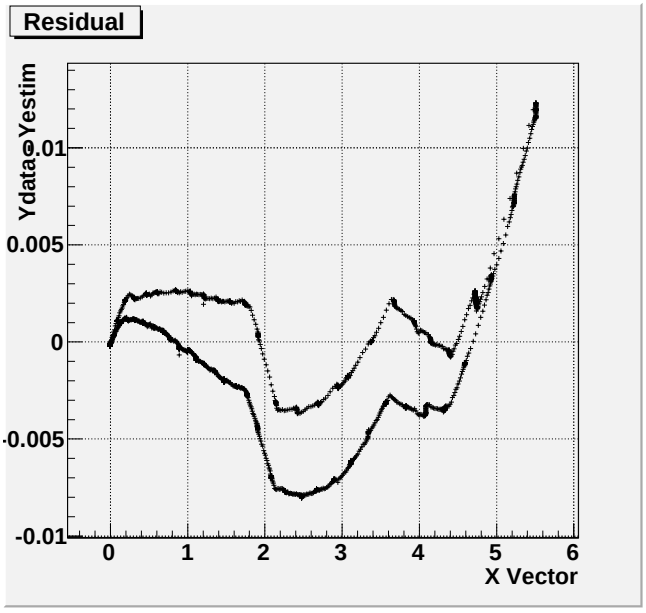

Figure 38: Residual plot #5 of Fermionics 2

C Fermionics 3

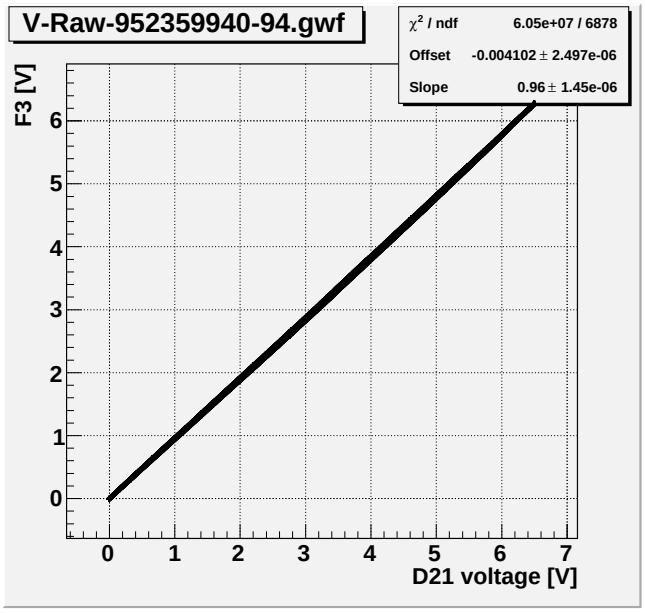

Figure 39: Linear fit #1 of Fermionics 3

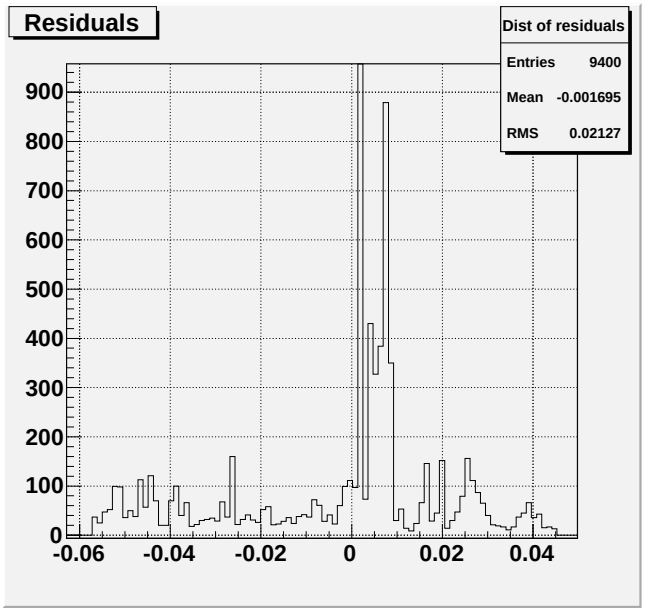

Figure 40: Residual distribution #1 of Fermionics 3

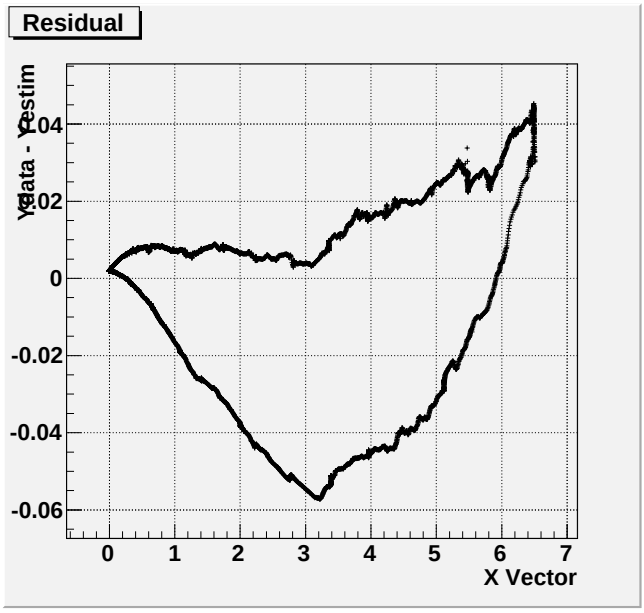

Figure 41: Residual plot #1 of Fermionics 3

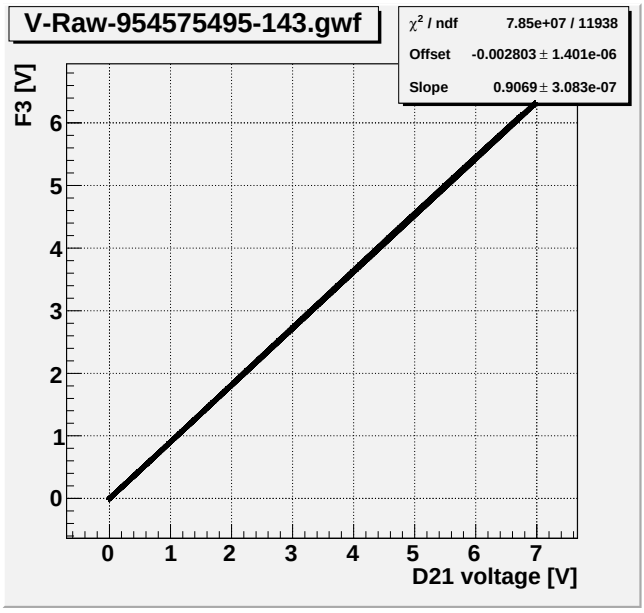

Figure 42: Linear fit #2 of Fermionics 3

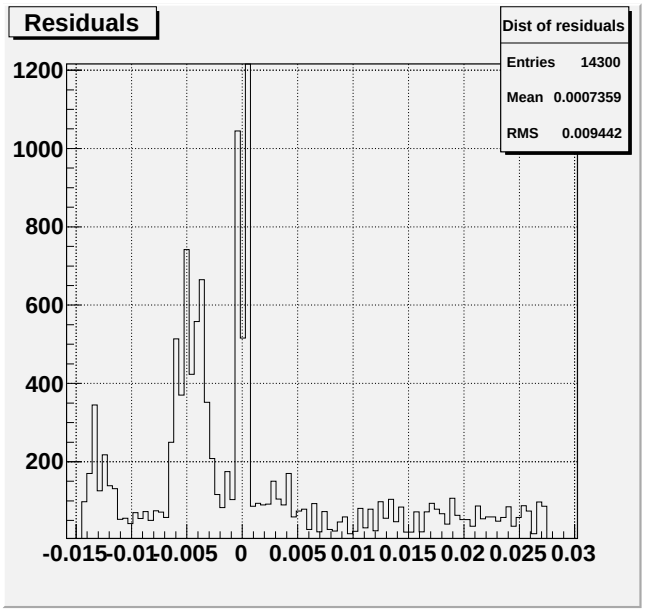

Figure 43: Residual distribution #2 of Fermionics 3

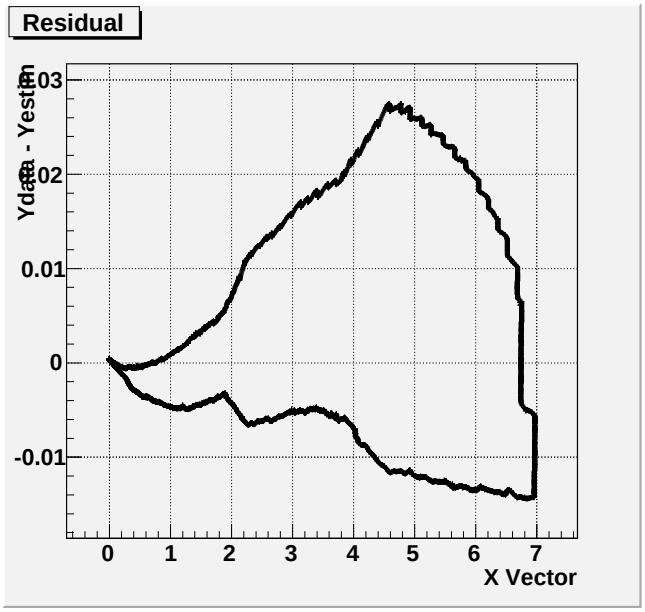

Figure 44: Residual plot #2 of Fermionics 3

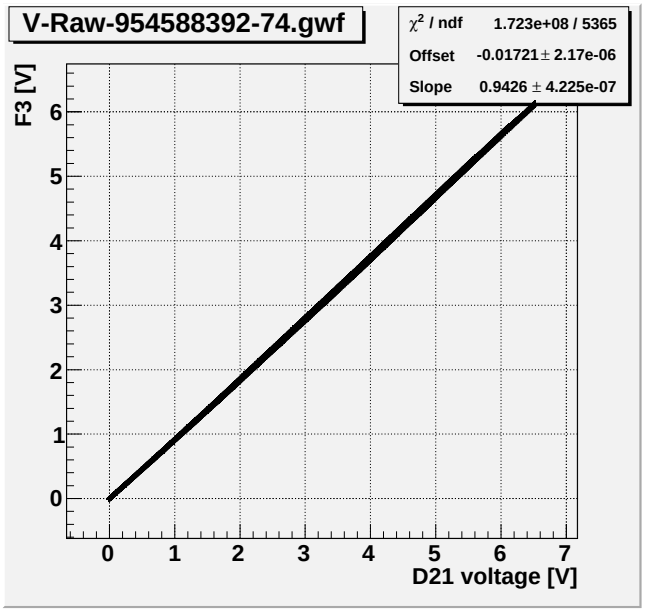

Figure 45: Linear fit #3 of Fermionics 3

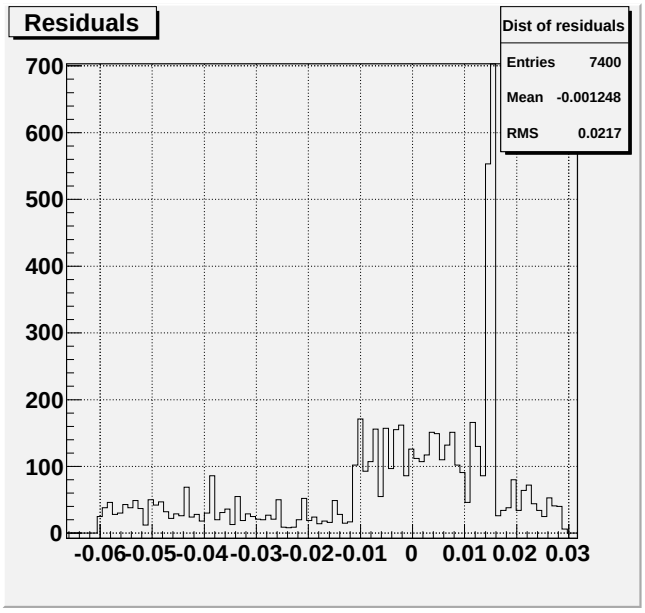

Figure 46: Residual distribution #3 of Fermionics 3

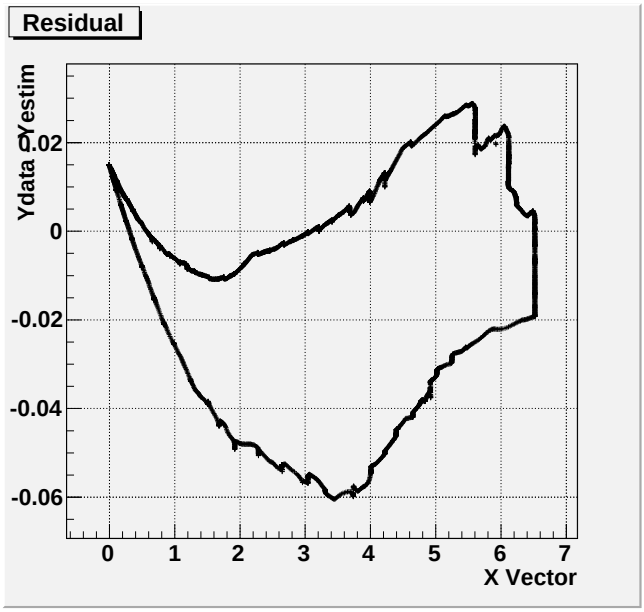

Figure 47: Residual plot #3 of Fermionics 3

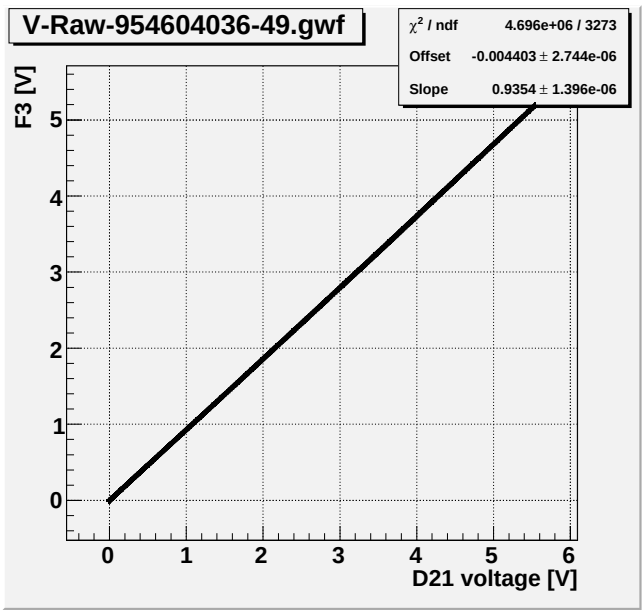

Figure 48: Linear fit #4 of Fermionics 3

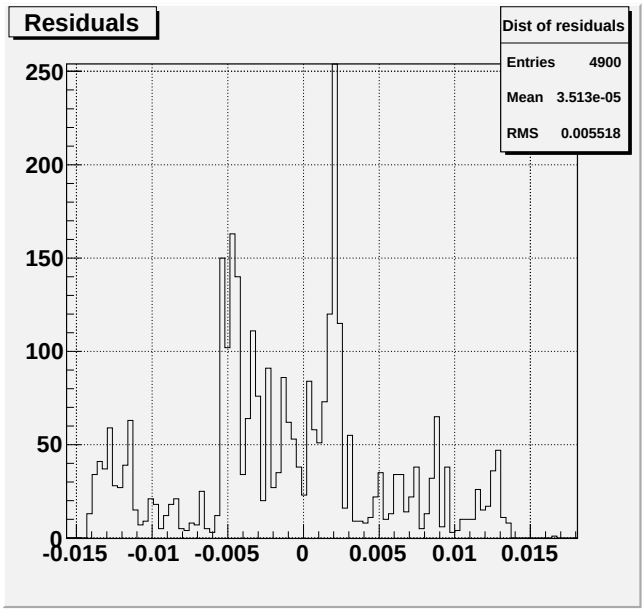

Figure 49: Residual distribution #4 of Fermionics 3

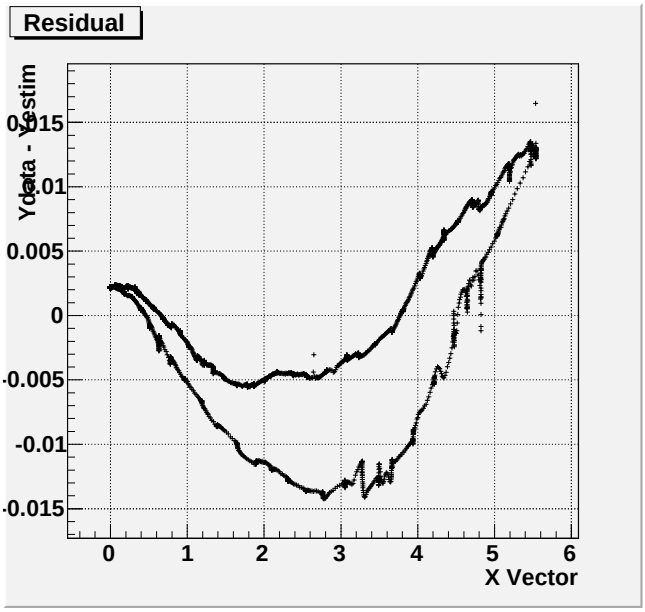

Figure 50: Residual plot #4 of Fermionics 3

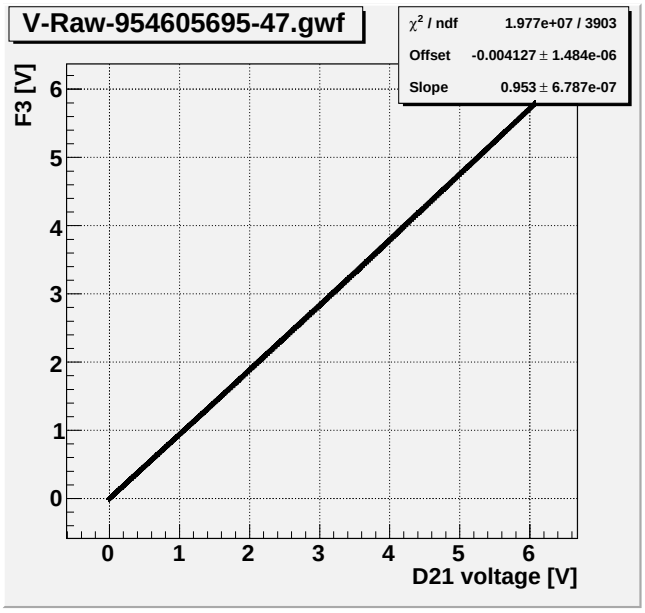

Figure 51: Linear fit #5 of Fermionics 3

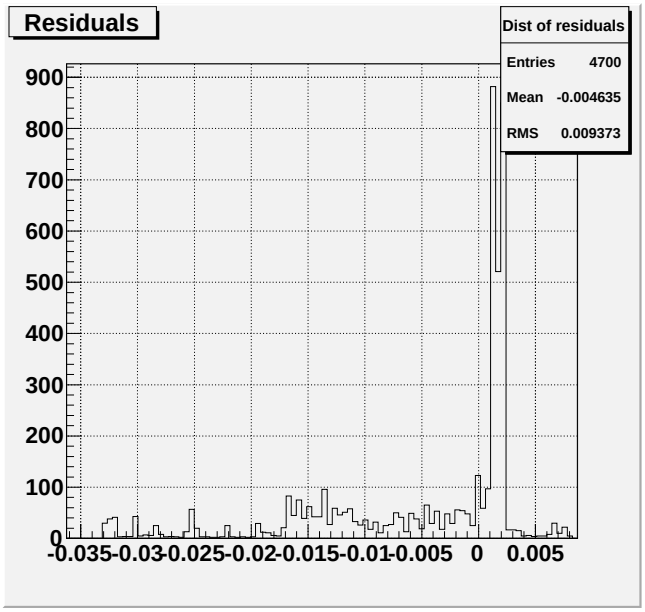

Figure 52: Residual distribution #5 of Fermionics 3

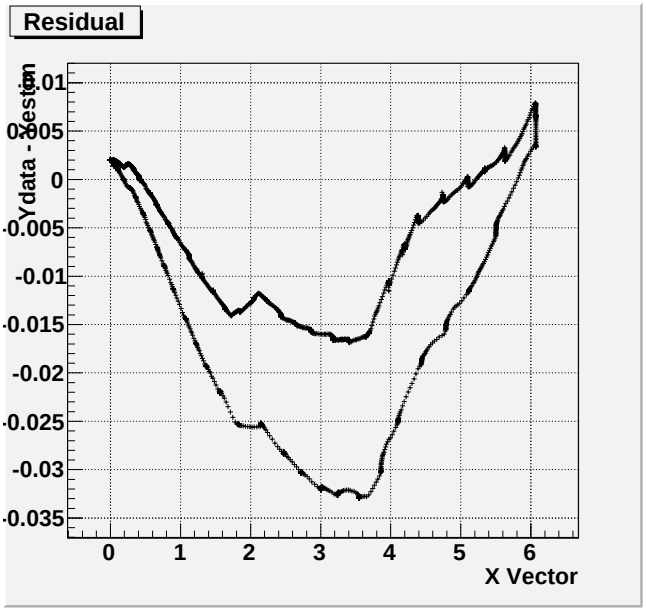

Figure 53: Residual plot #5 of Fermionics 3

D Judson 1

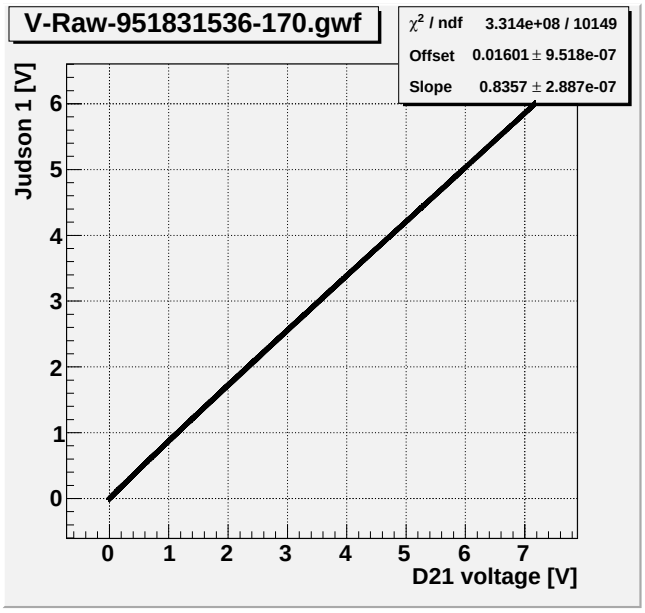

Figure 54: Linear fit #1 of Judson 1

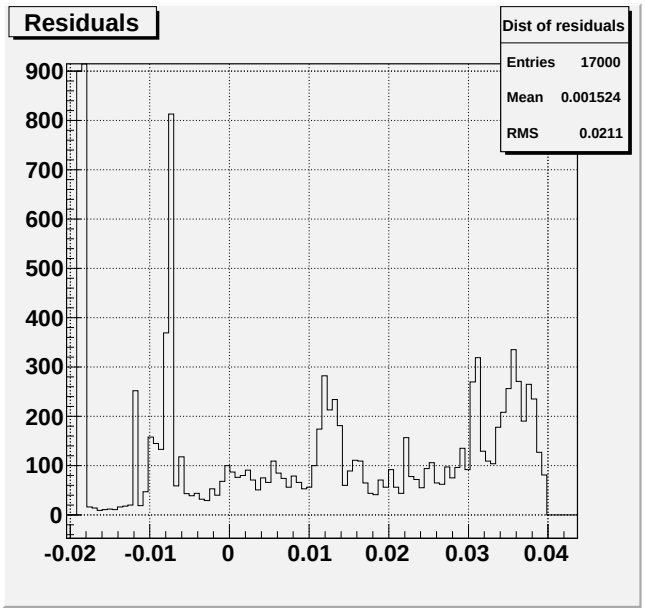

Figure 55: Residual distribution #1 of Judson 1

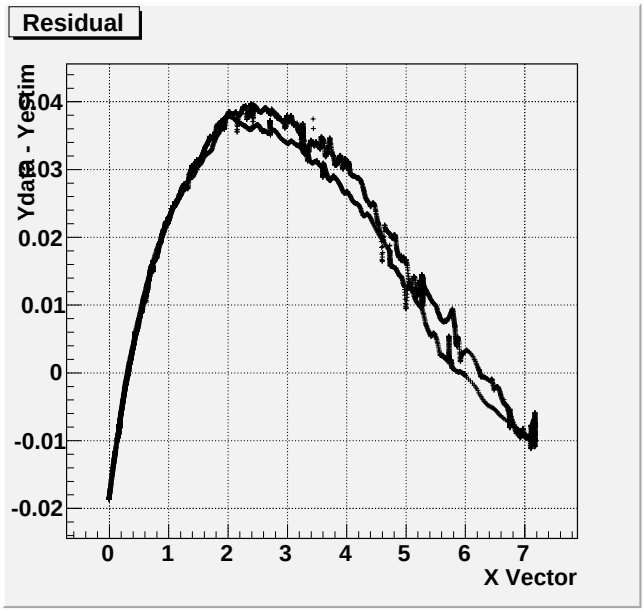

Figure 56: Residual plot #1 of Judson 1

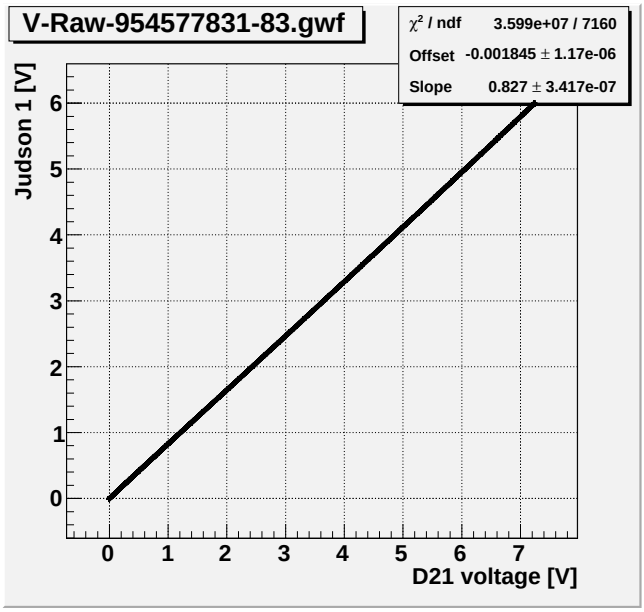

Figure 57: Linear fit #2 of Judson 1

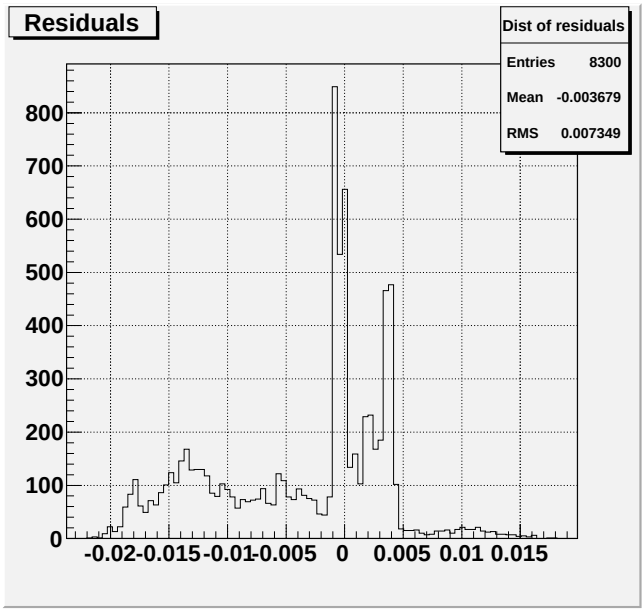

Figure 58: Residual distribution #2 of Judson 1

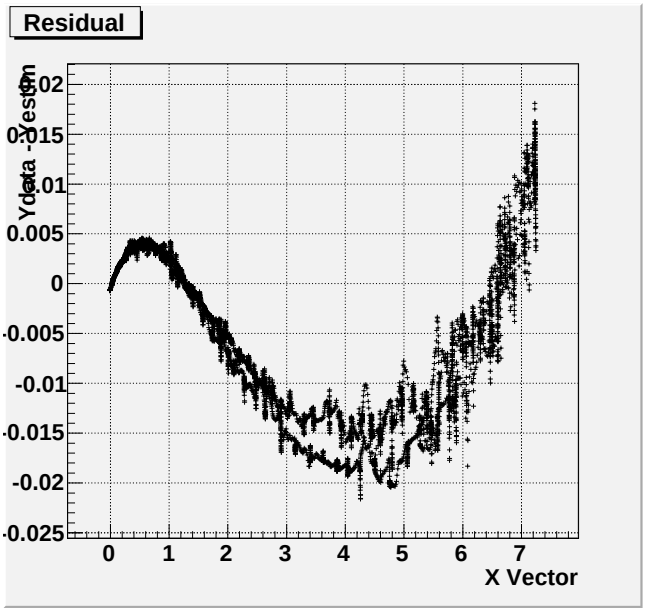

Figure 59: Residual plot #2 of Judson 1

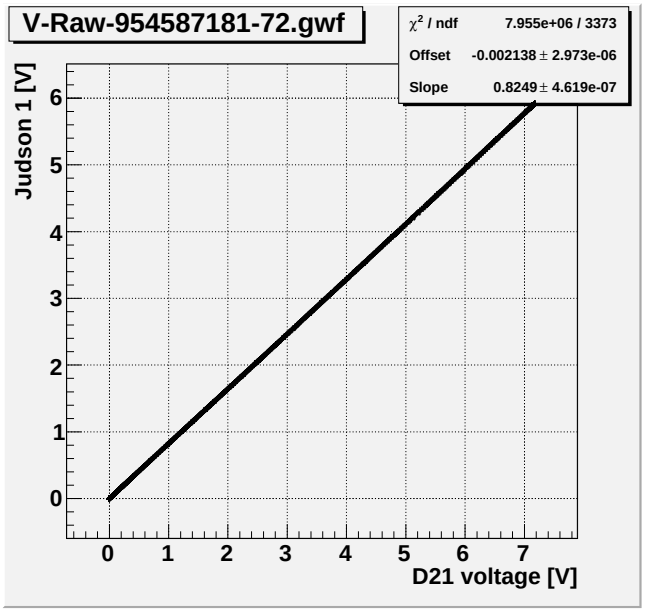

Figure 60: Linear fit #3 of Judson 1

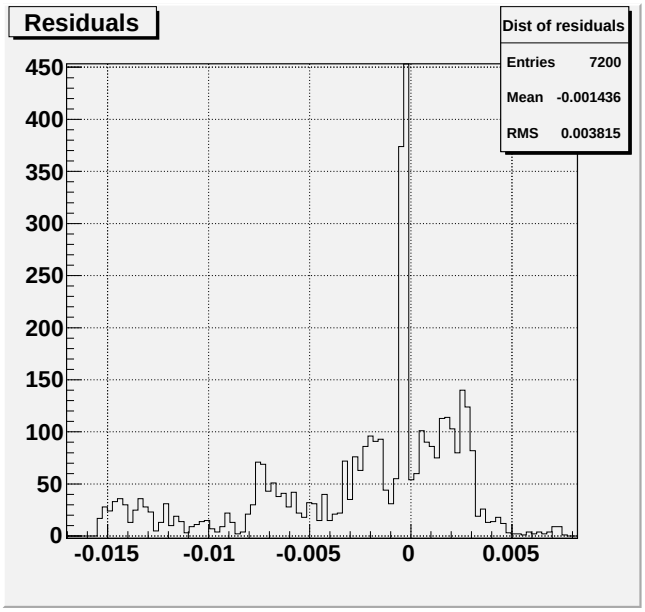

Figure 61: Residual distribution #3 of Judson 1

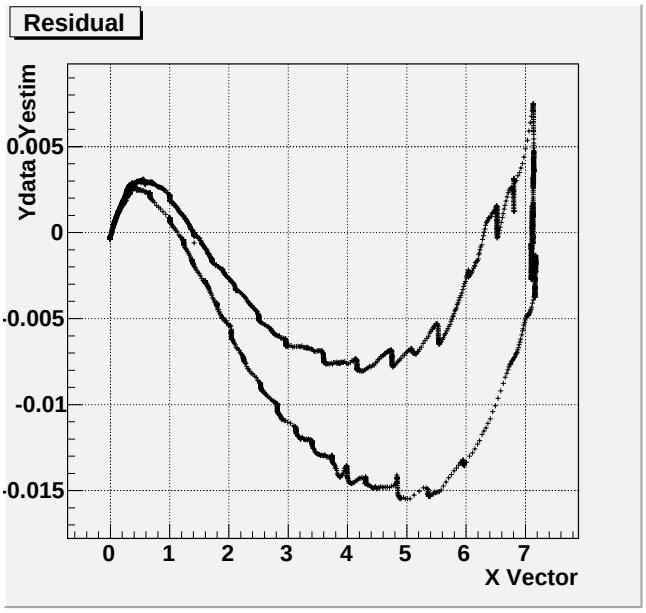

Figure 62: Residual plot #3 of Judson 1

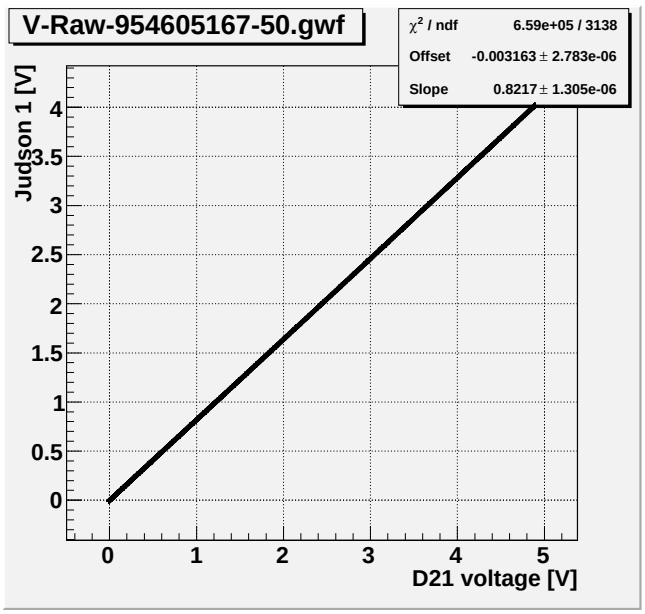

Figure 63: Linear fit #4 of Judson 1

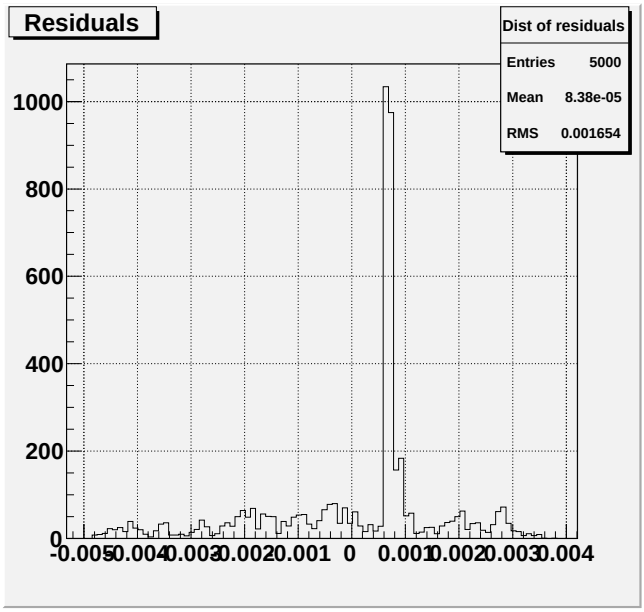

Figure 64: Residual distribution #4 of Judson 1

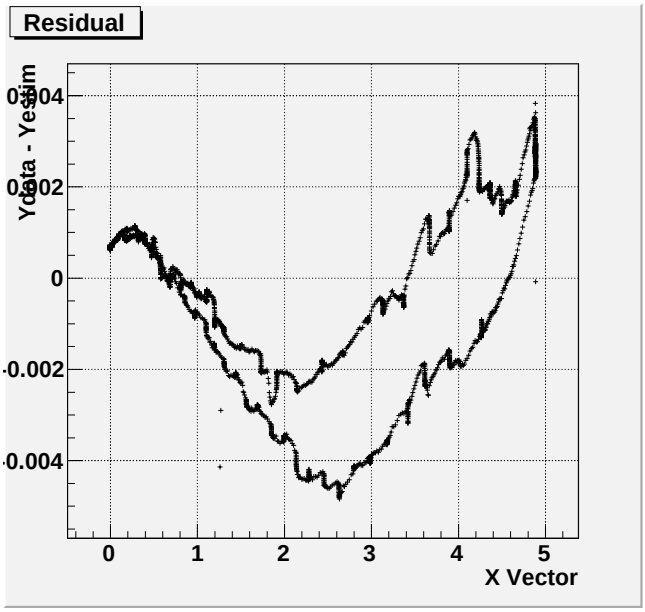

Figure 65: Residual plot #4 of Judson 1

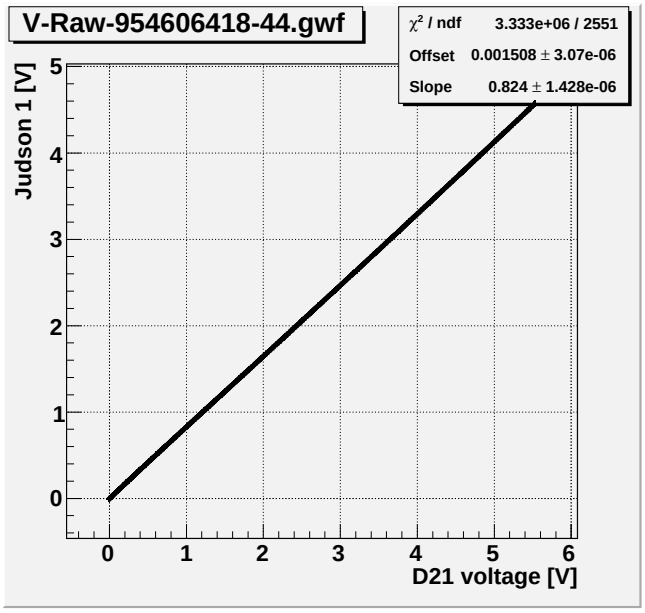

Figure 66: Linear fit #5 of Judson 1

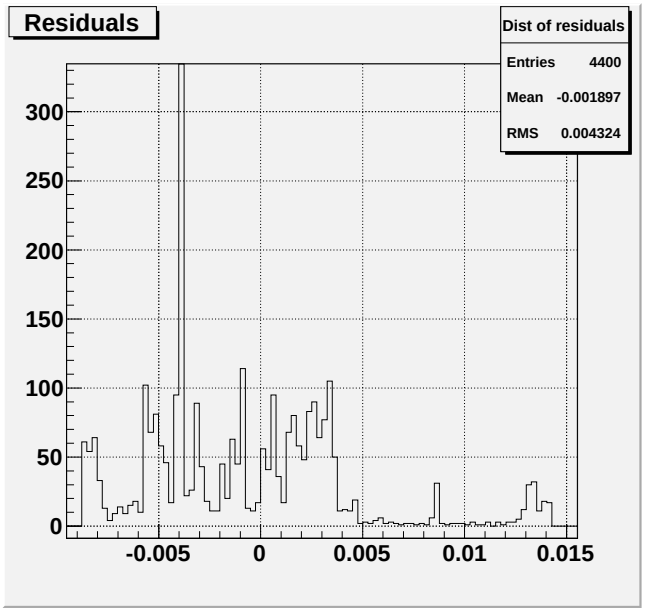

Figure 67: Residual distribution #5 of Judson 1

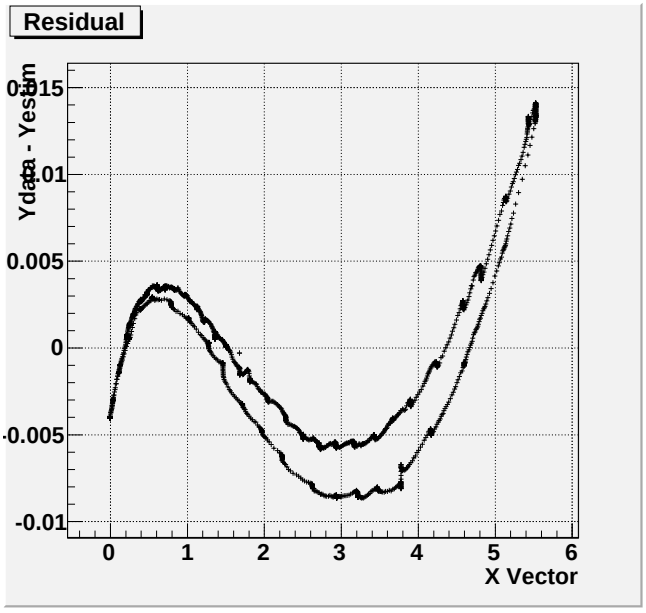

Figure 68: Residual plot #5 of Judson 1

E Judson 2

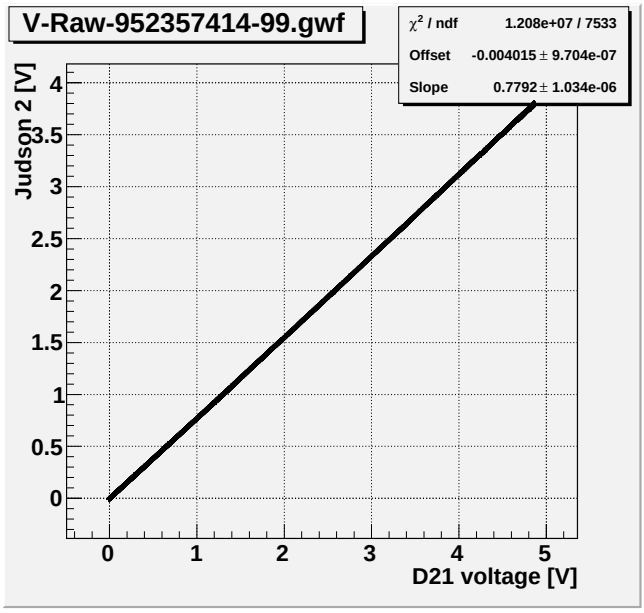

Figure 69: Linear fit #1 of Judson 2

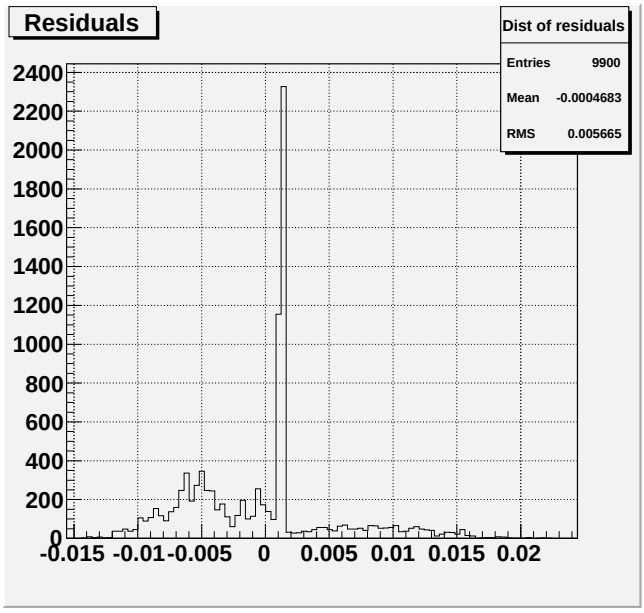

Figure 70: Residual distribution #1 of Judson 2

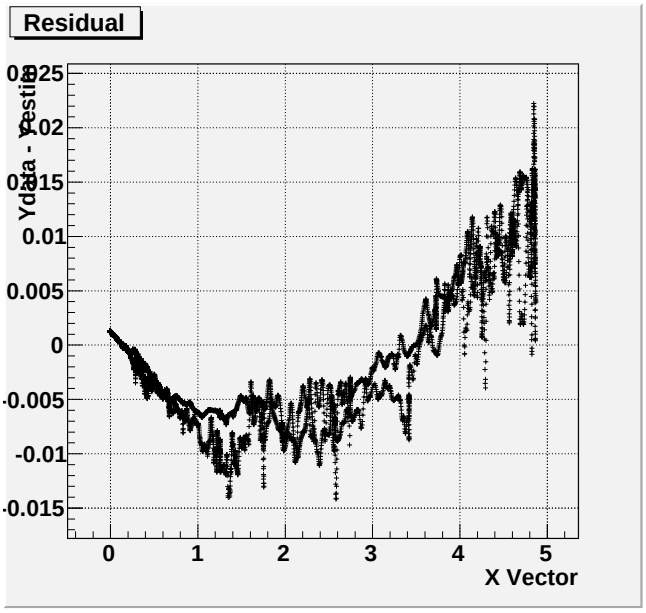

Figure 71: Residual plot #1 of Judson 2

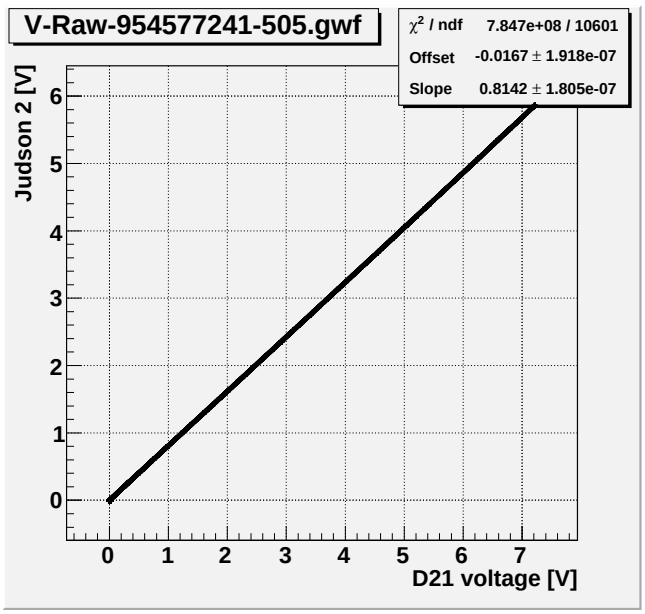

Figure 72: Linear fit #2 of Judson 2

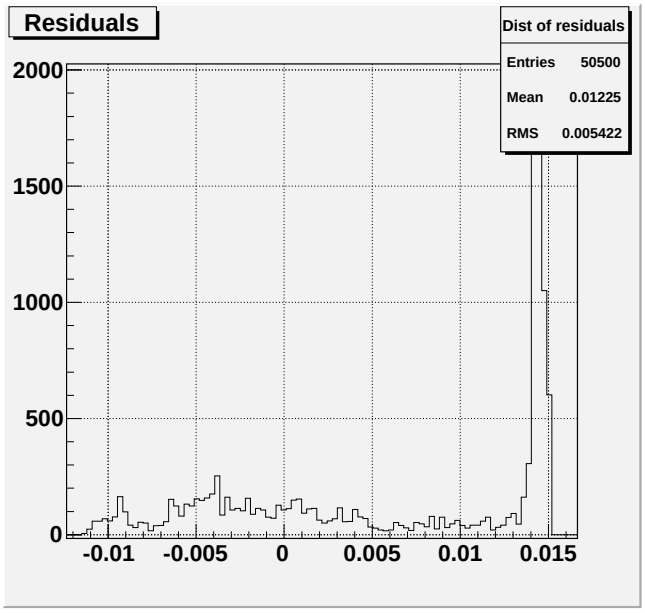

Figure 73: Residual distribution #2 of Judson 2

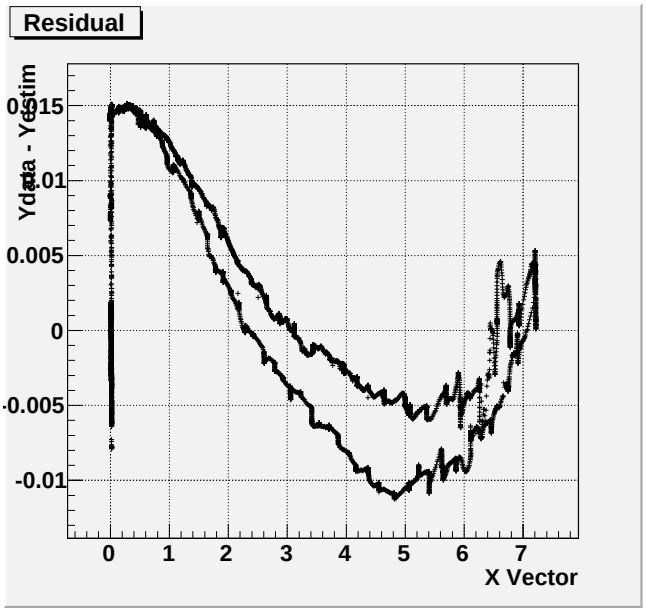

Figure 74: Residual plot #2 of Judson 2

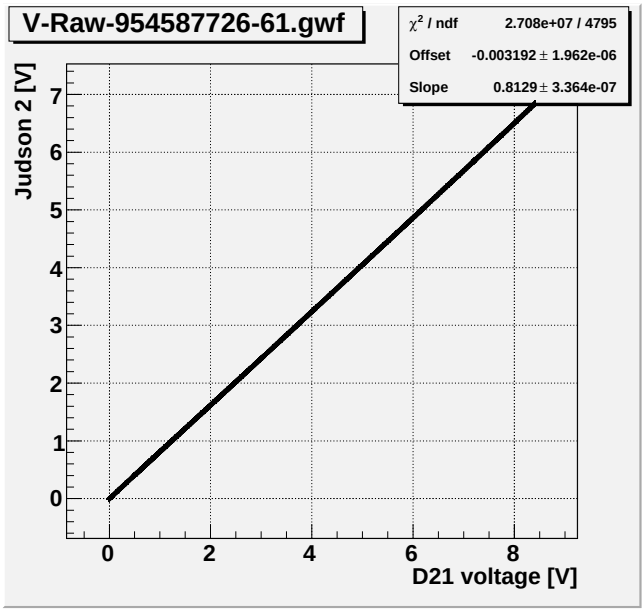

Figure 75: Linear fit #3 of Judson 2

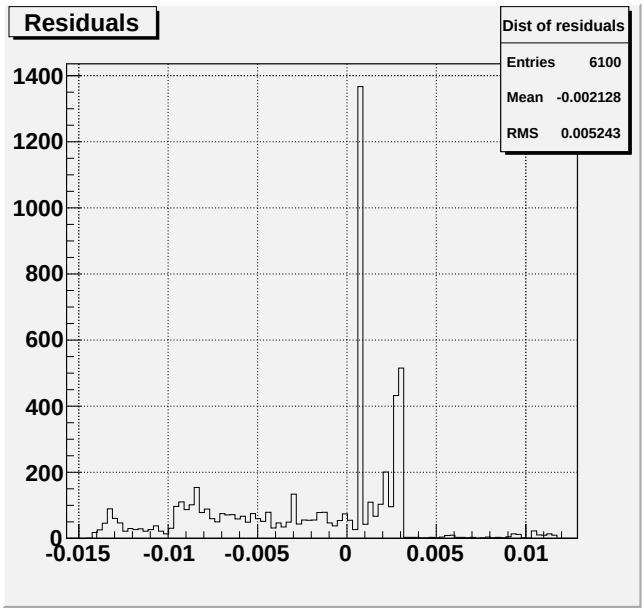

Figure 76: Residual distribution #3 of Judson 2

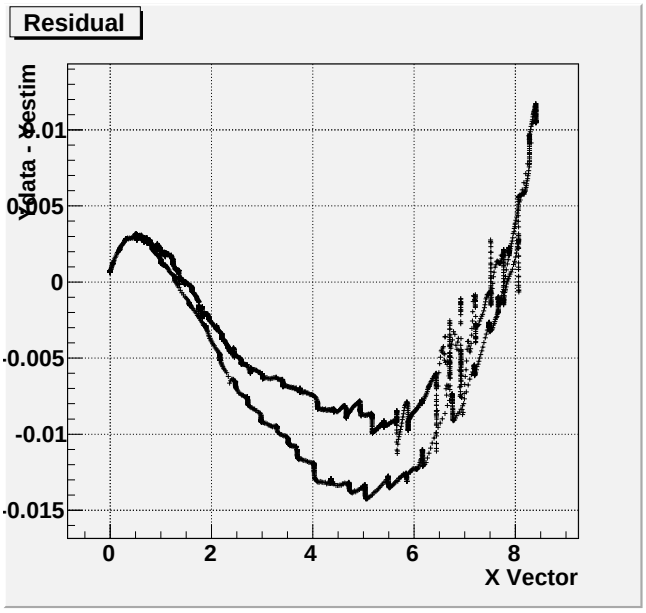

Figure 77: Residual plot #3 of Judson 2

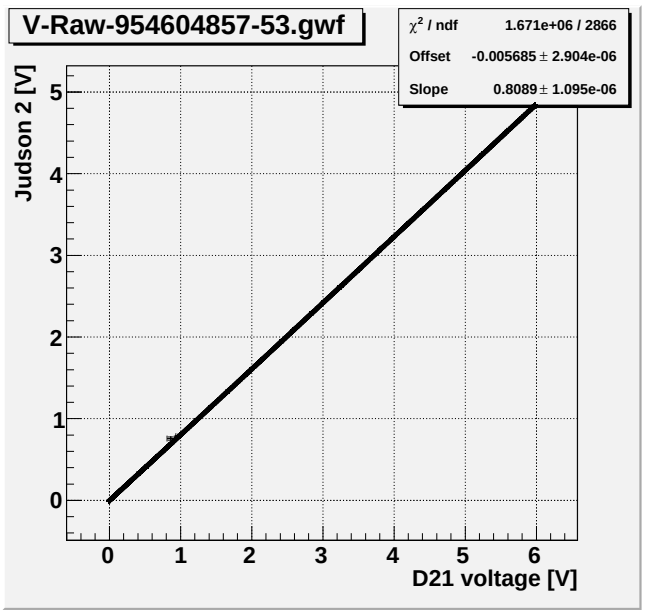

Figure 78: Linear fit #4 of Judson 2

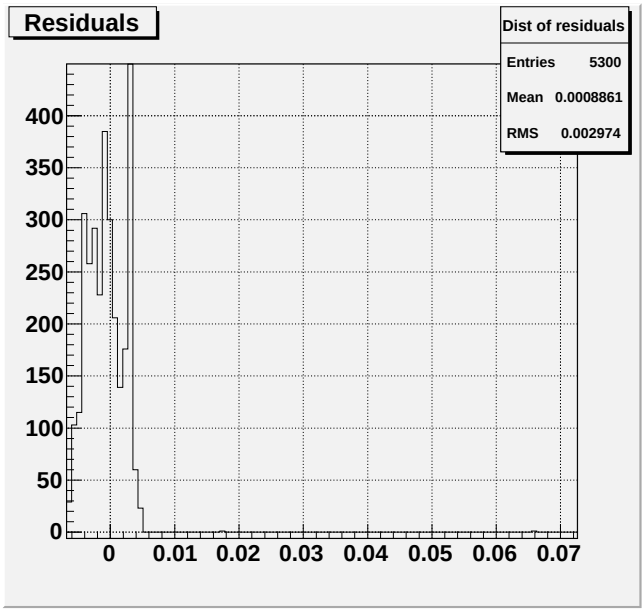

Figure 79: Residual distribution #4 of Judson 2

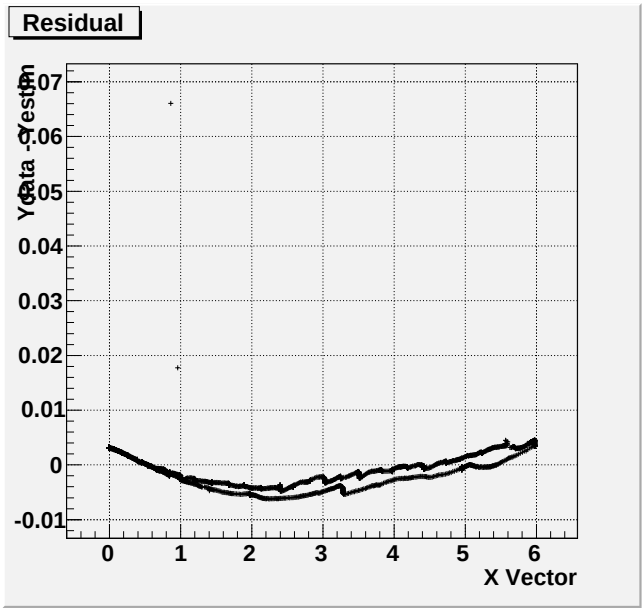

Figure 80: Residual plot #4 of Judson 2

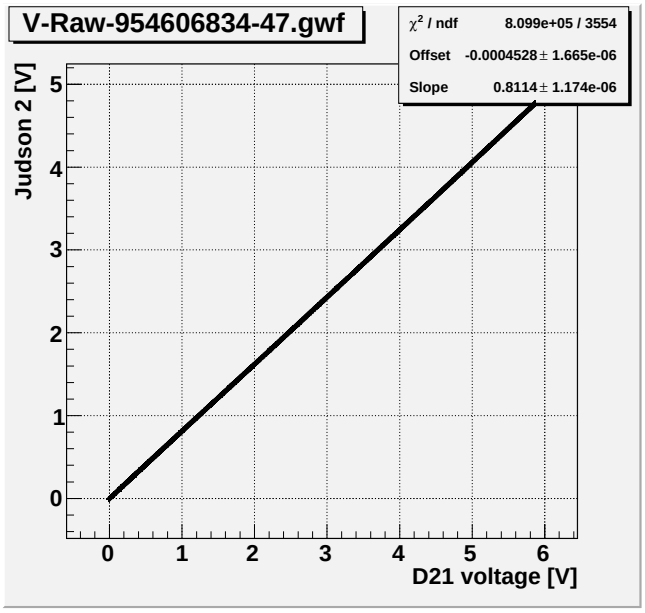

Figure 81: Linear fit #5 of Judson 2

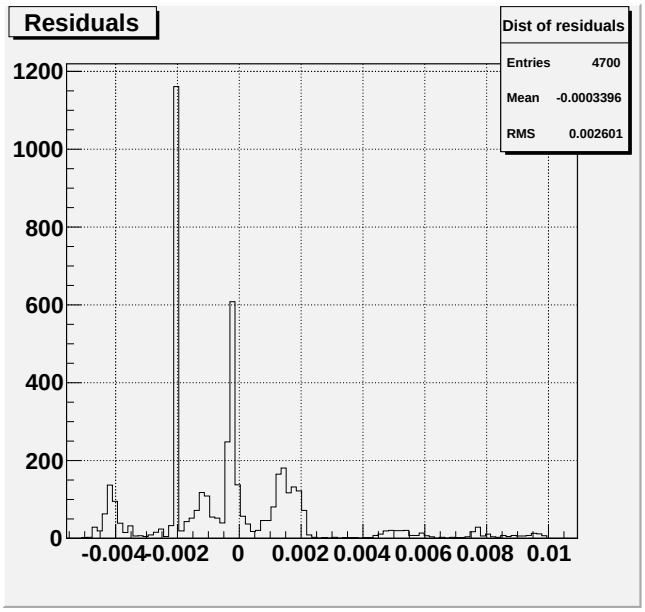

Figure 82: Residual distribution #5 of Judson 2

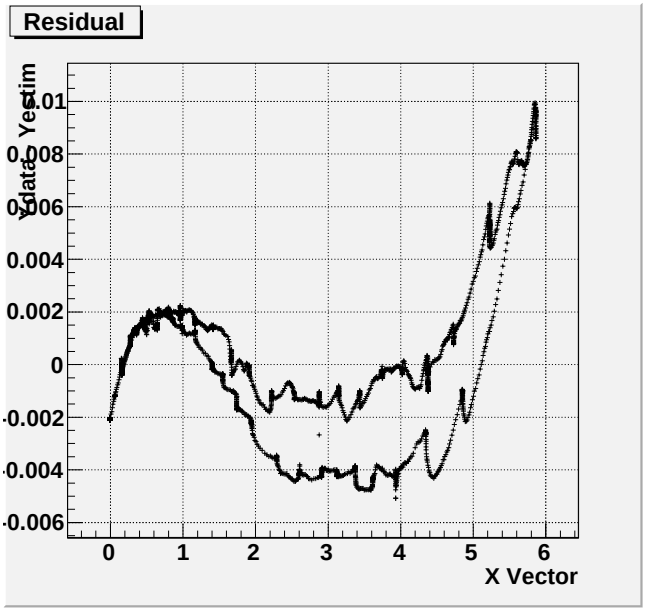

Figure 83: Residual plot #5 of Judson 2

F Perkin Elmer 94

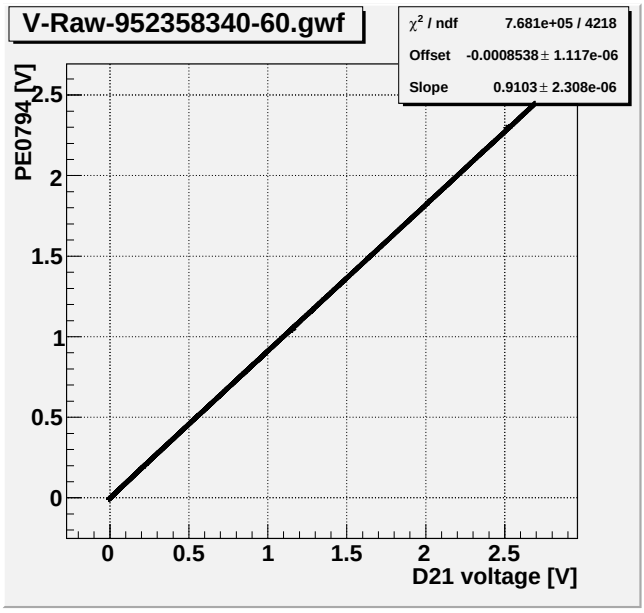

Figure 84: Linear fit #1 of Perkin Elmer 94

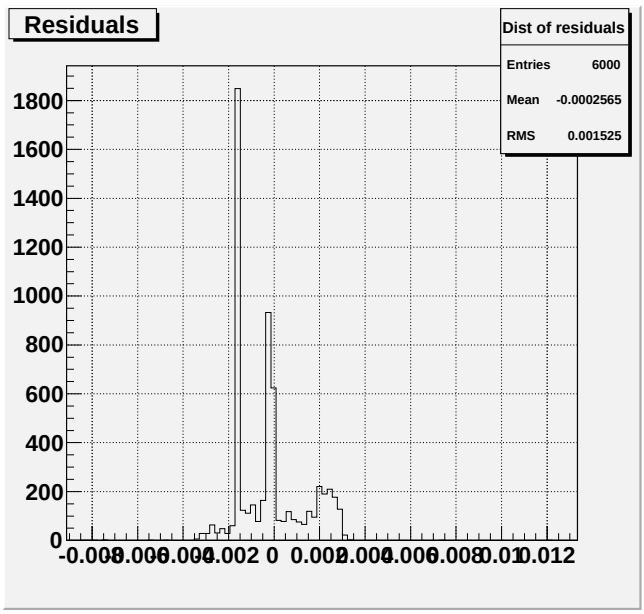

Figure 85: Residual distribution #1 of Perkin Elmer 94

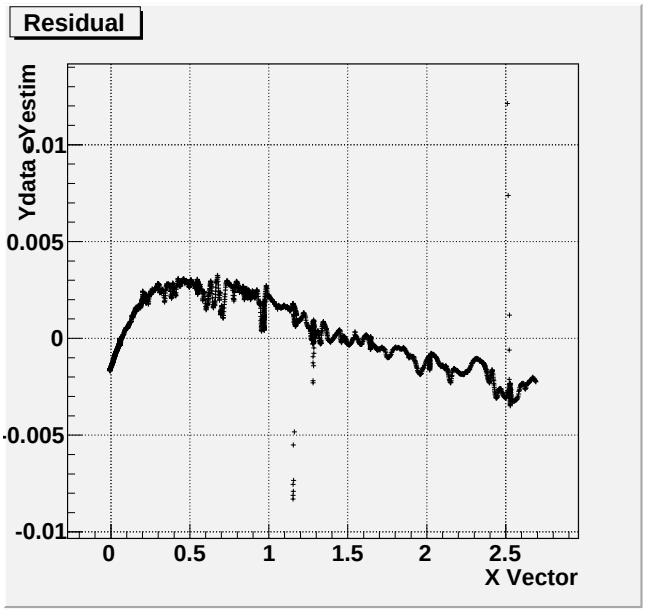

Figure 86: Residual plot #1 of Perkin Elmer 94

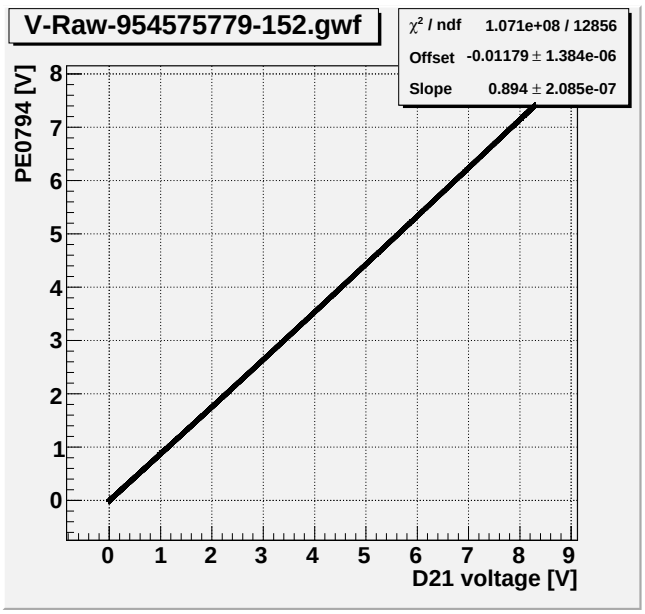

Figure 87: Linear fit #2 of Perkin Elmer 94

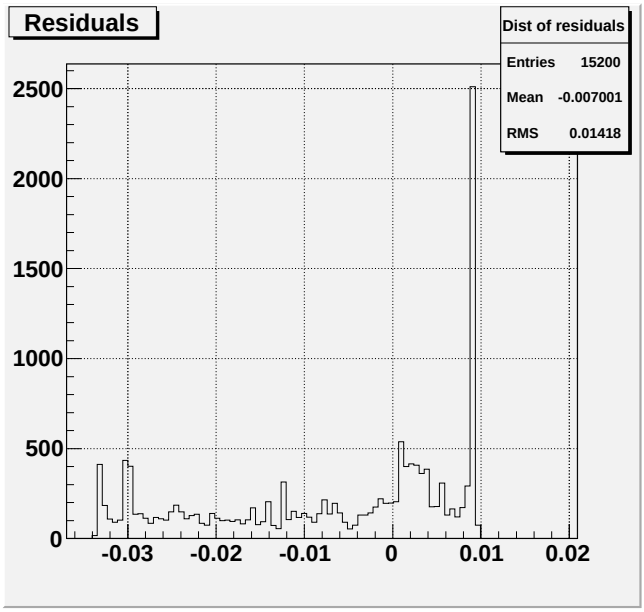

Figure 88: Residual distribution #2 of Perkin Elmer 94

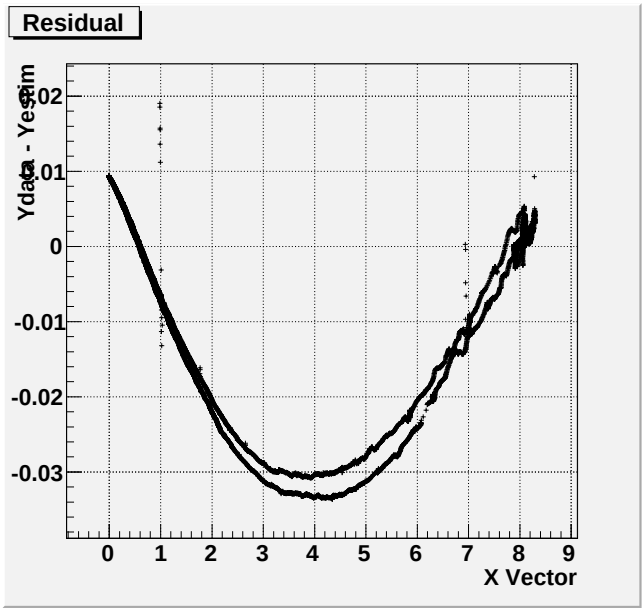

Figure 89: Residual plot #2 of Perkin Elmer 94

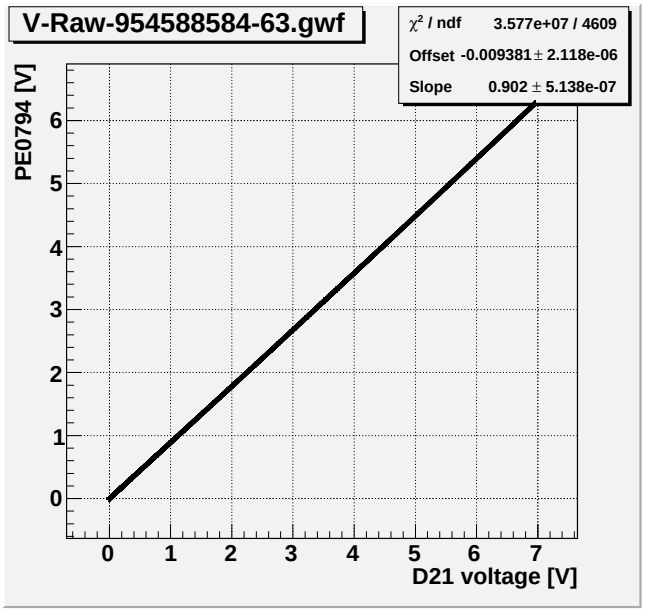

Figure 90: Linear fit #3 of Perkin Elmer 94

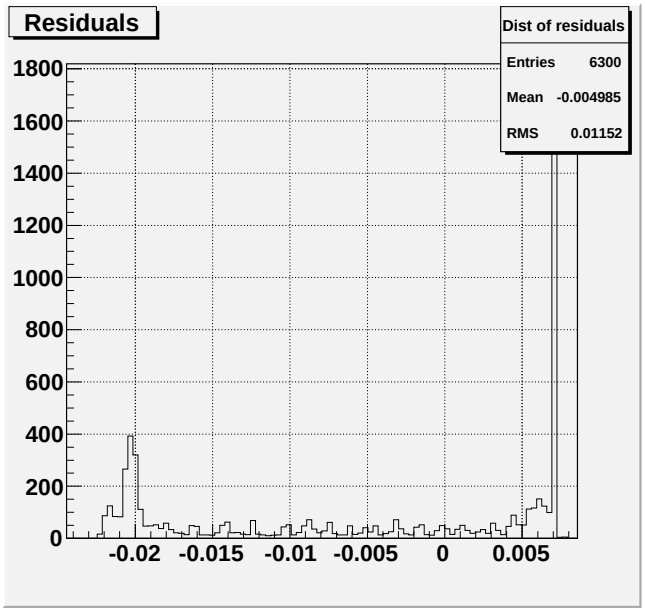

Figure 91: Residual distribution #3 of Perkin Elmer 94

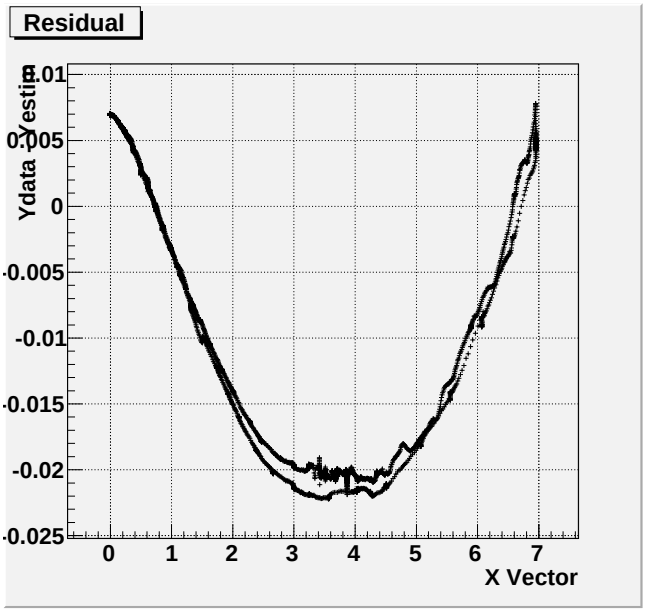

Figure 92: Residual plot #3 of Perkin Elmer 94

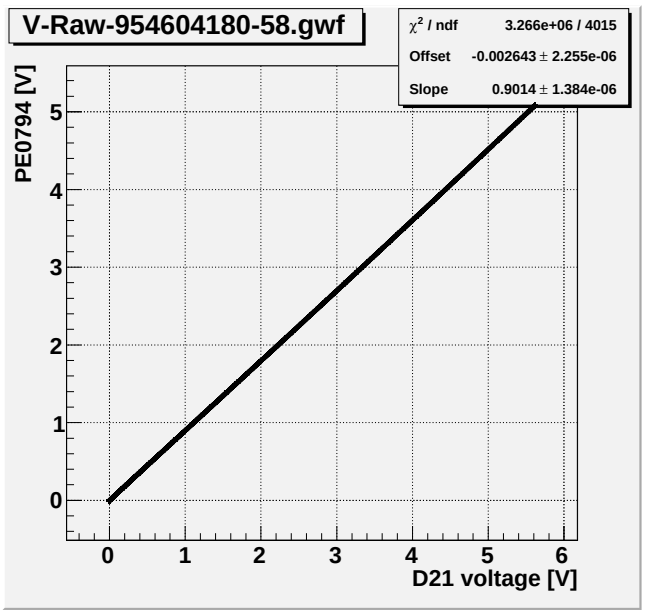

Figure 93: Linear fit #4 of Perkin Elmer 94

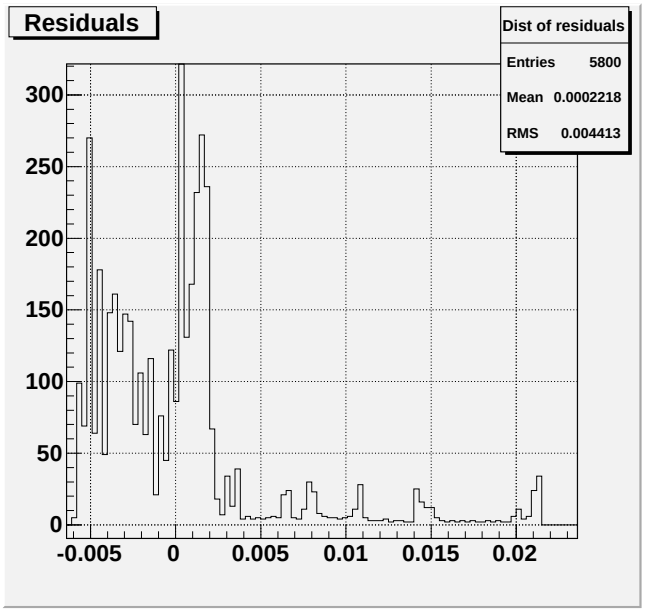

Figure 94: Residual distribution #4 of Perkin Elmer 94

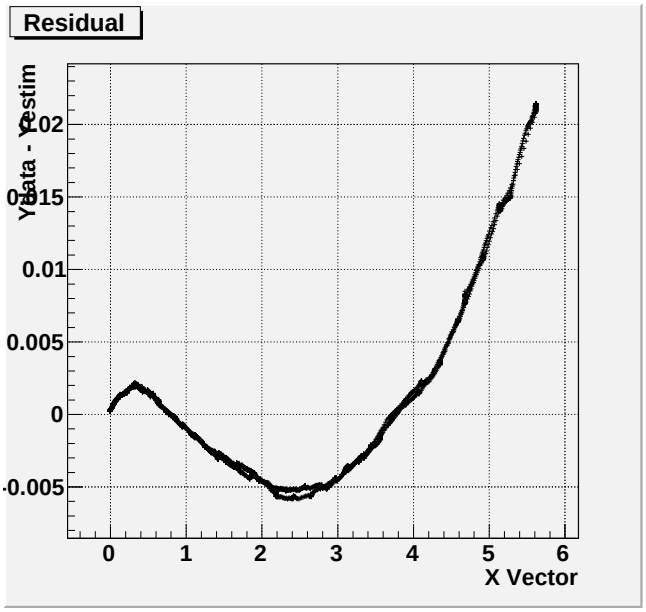

Figure 95: Residual plot #4 of Perkin Elmer 94

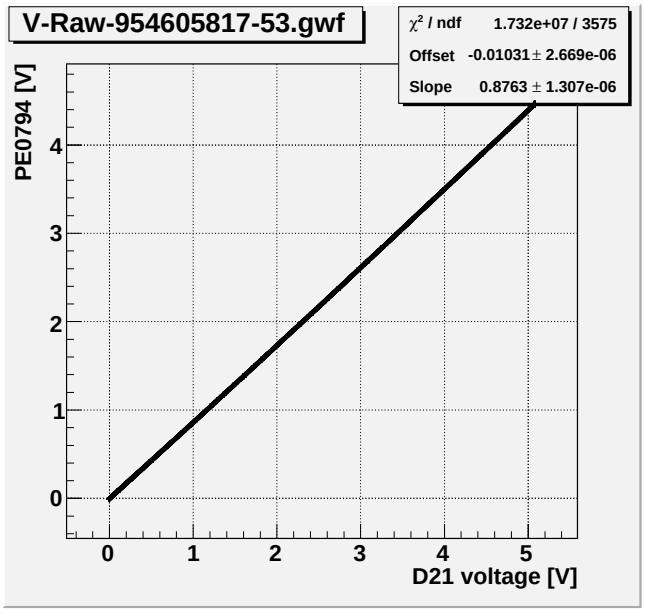

Figure 96: Linear fit #5 of Perkin Elmer 94

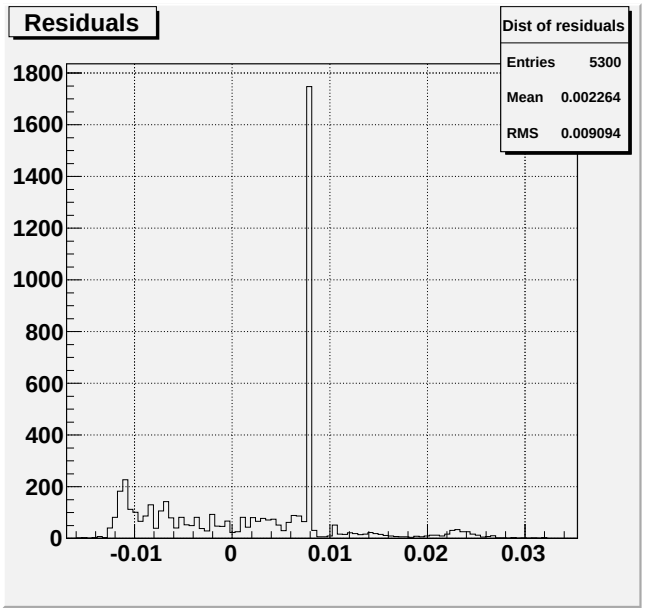

Figure 97: Residual distribution #5 of Perkin Elmer 94

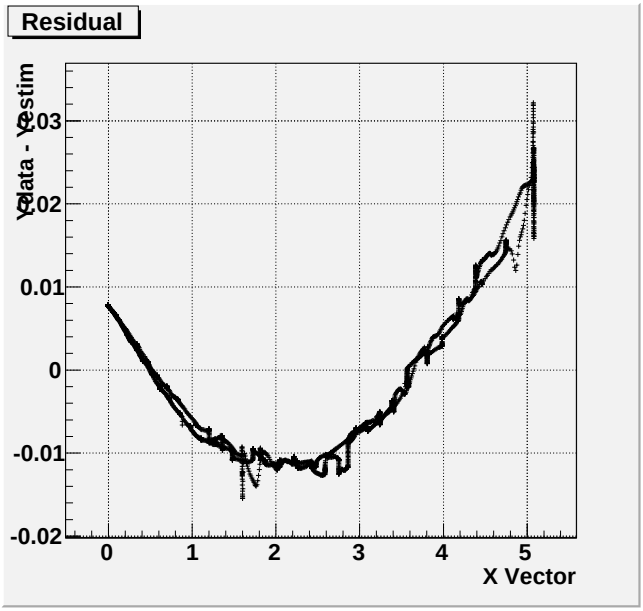

Figure 98: Residual plot #5 of Perkin Elmer 94

G Perkin Elmer 95

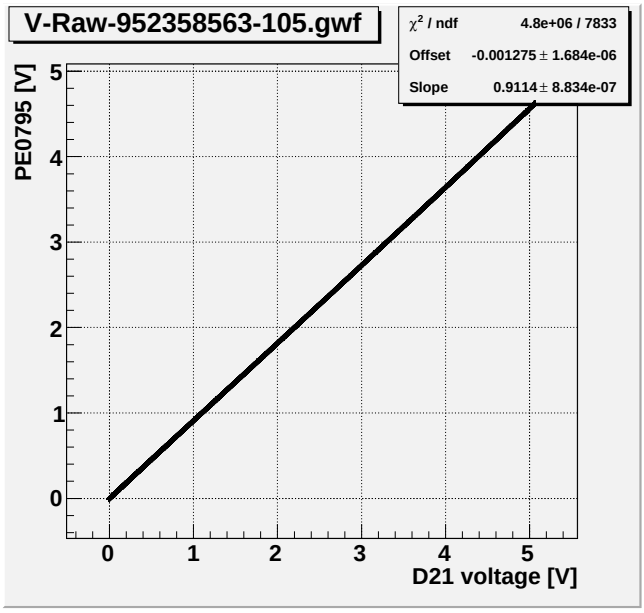

Figure 99: Linear fit #1 of Perkin Elmer 95

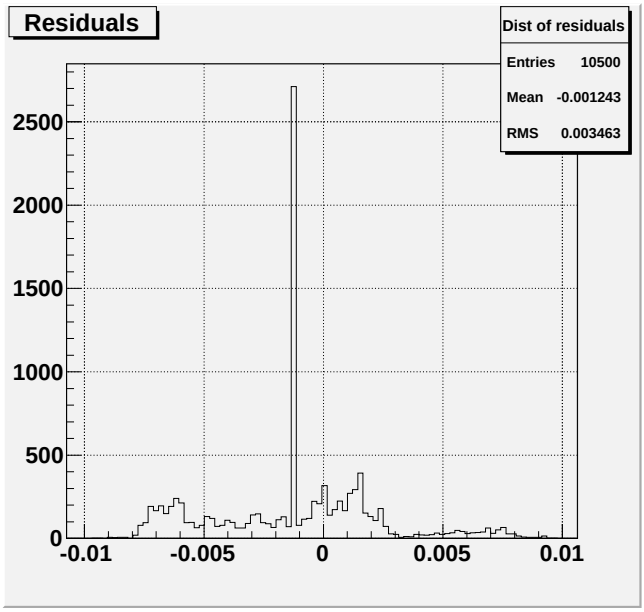

Figure 100: Residual distribution #1 of Perkin Elmer 95

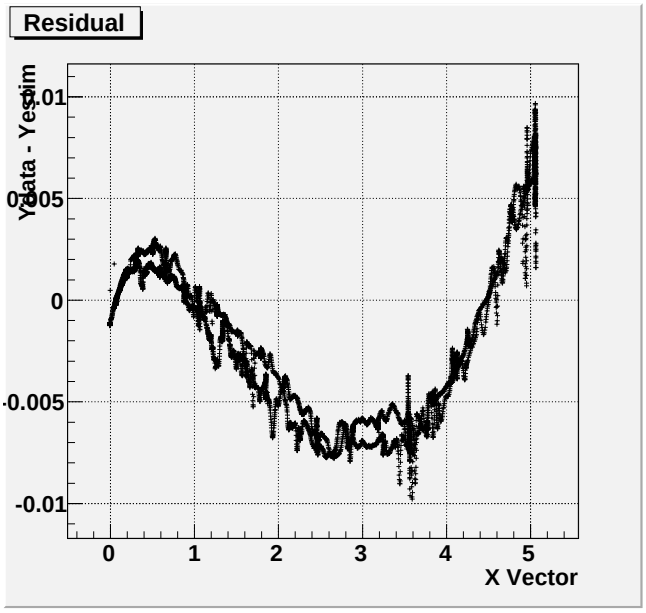

Figure 101: Residual plot #1 of Perkin Elmer 95

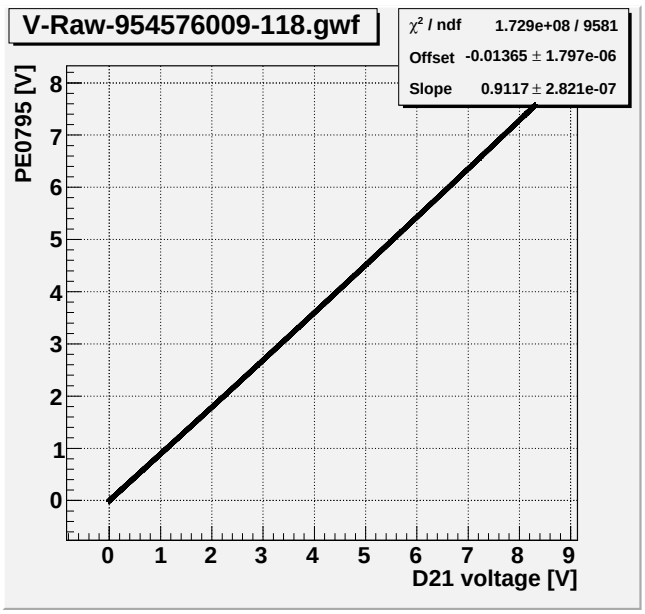

Figure 102: Linear fit #2 of Perkin Elmer 95

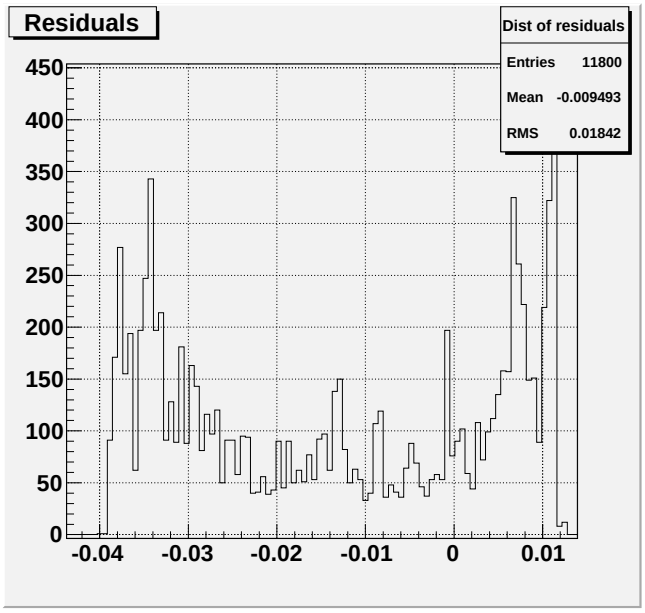

Figure 103: Residual distribution #2 of Perkin Elmer 95

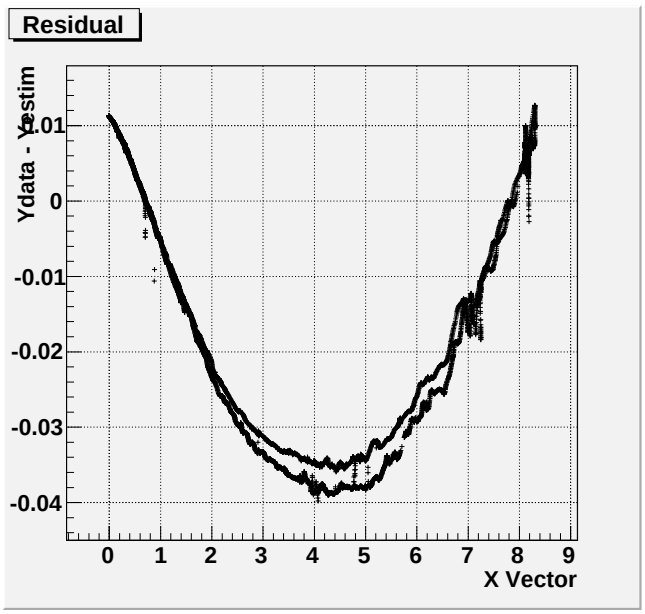

Figure 104: Residual plot #2 of Perkin Elmer 95

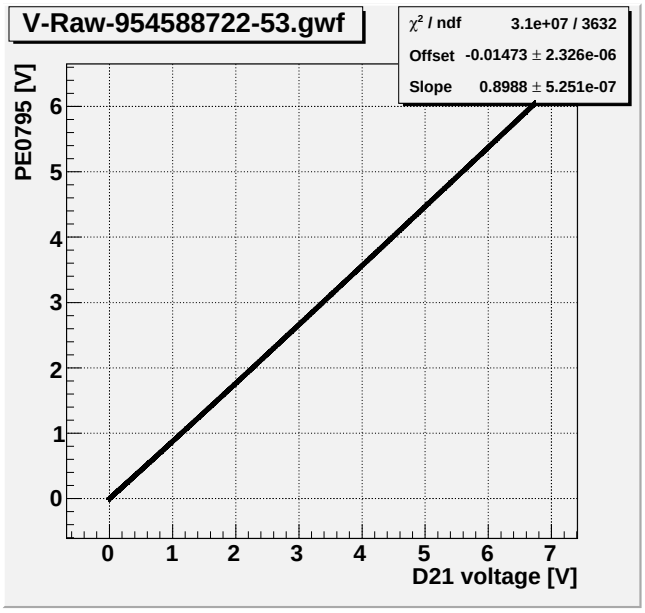

Figure 105: Linear fit #3 of Perkin Elmer 95

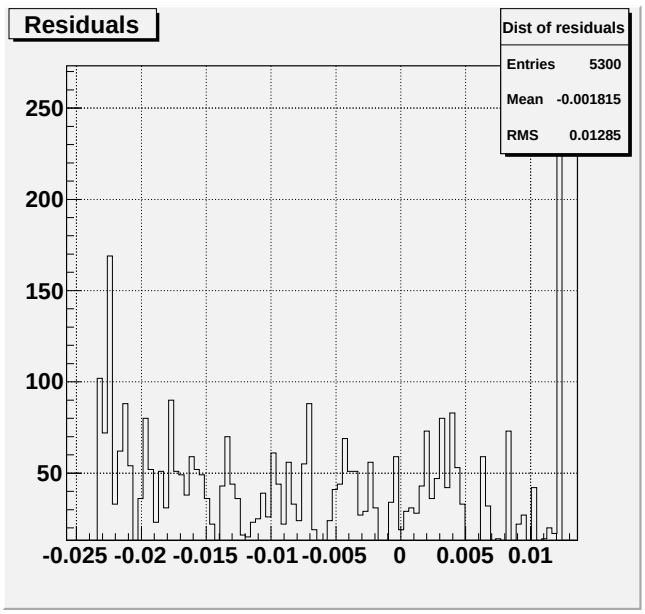

Figure 106: Residual distribution #3 of Perkin Elmer 95

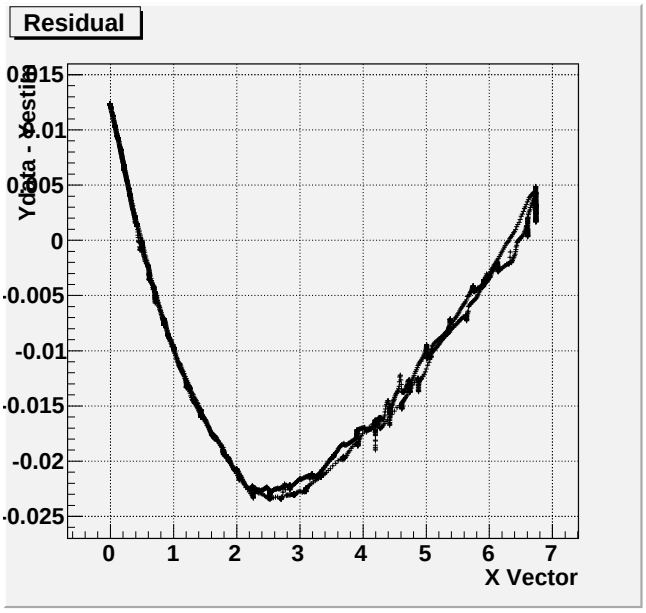

Figure 107: Residual plot #3 of Perkin Elmer 95

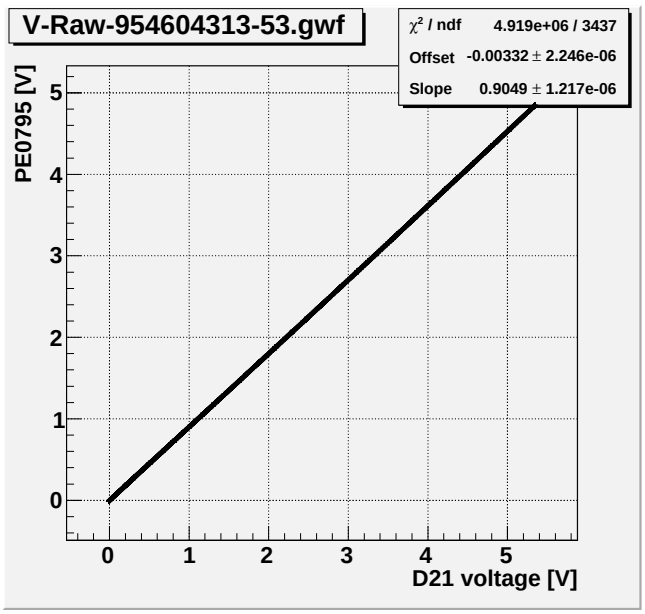

Figure 108: Linear fit #4 of Perkin Elmer 95

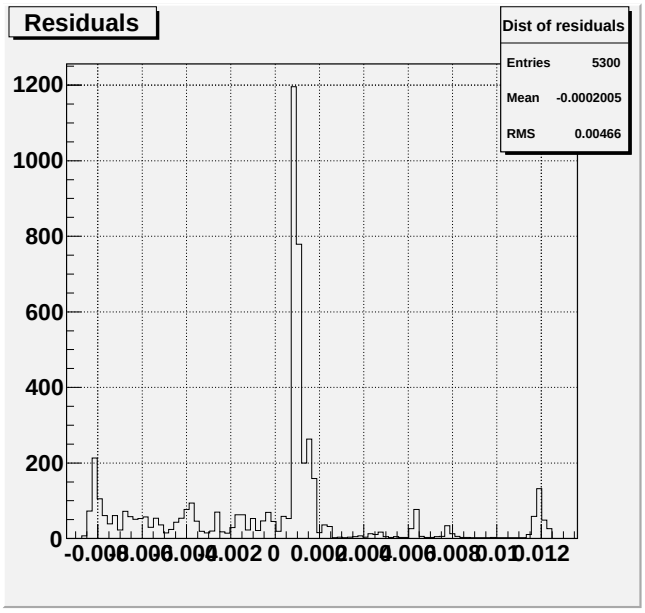

Figure 109: Residual distribution #4 of Perkin Elmer 95

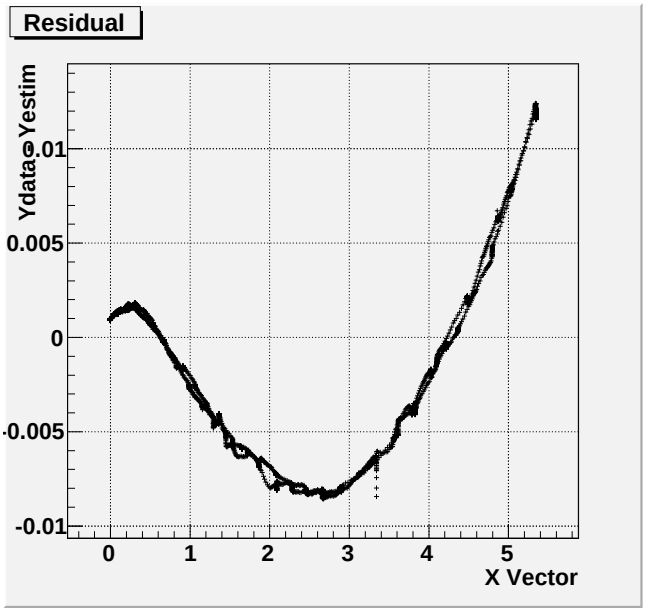

Figure 110: Residual plot #4 of Perkin Elmer 95

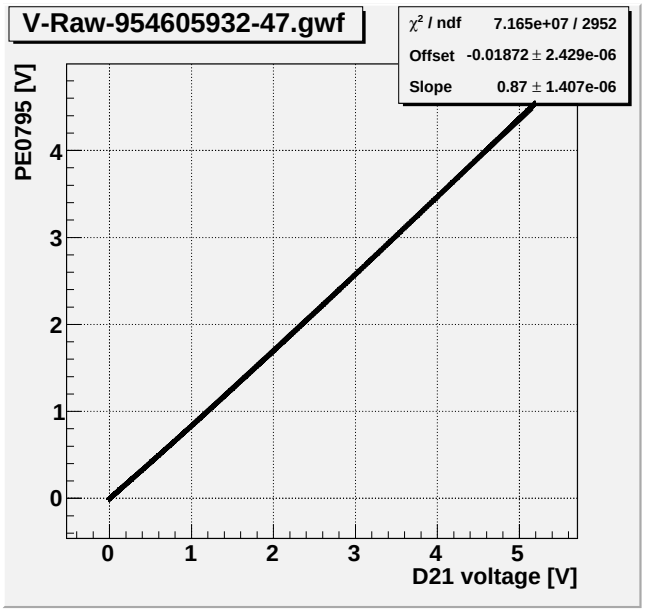

Figure 111: Linear fit #5 of Perkin Elmer 95

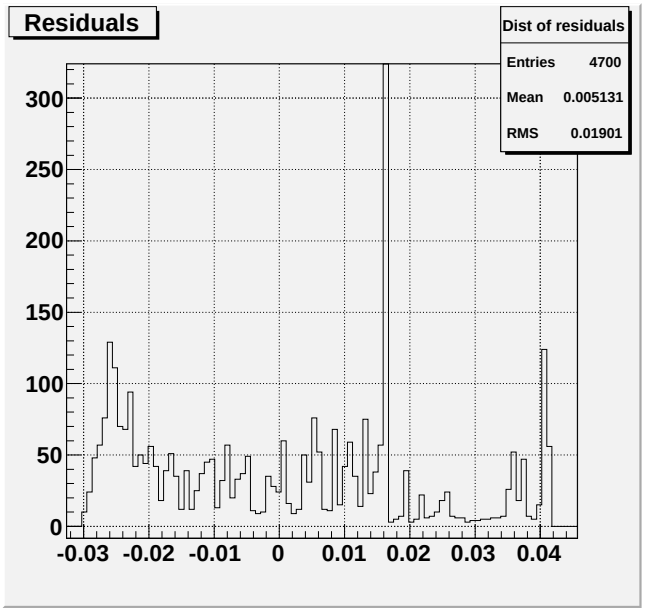

Figure 112: Residual distribution #5 of Perkin Elmer 95

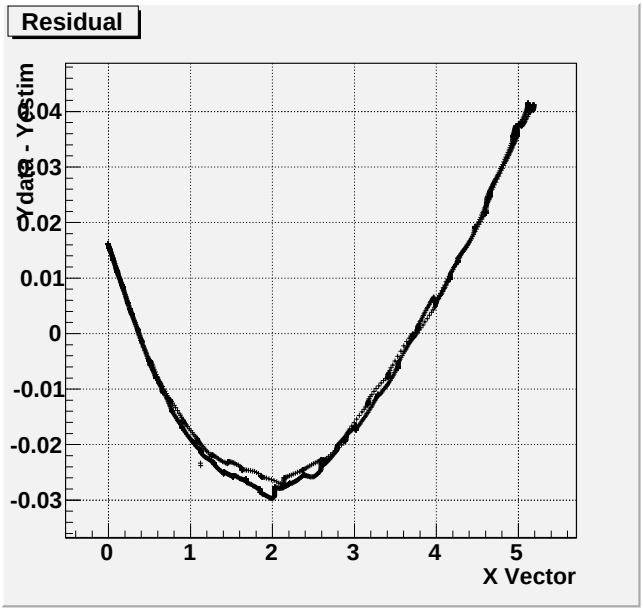

Figure 113: Residual plot #5 of Perkin Elmer 95

H Perkin Elmer 96

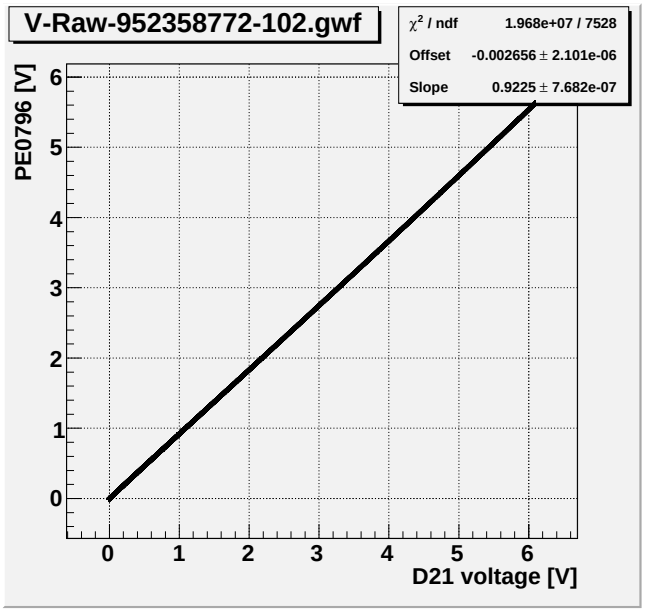

Figure 114: Linear fit #1 of Perkin Elmer 96

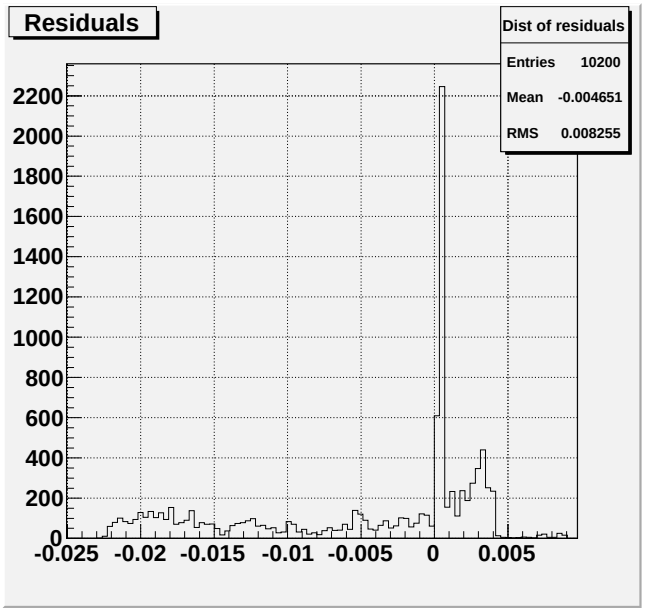

Figure 115: Residual distribution #1 of Perkin Elmer 96

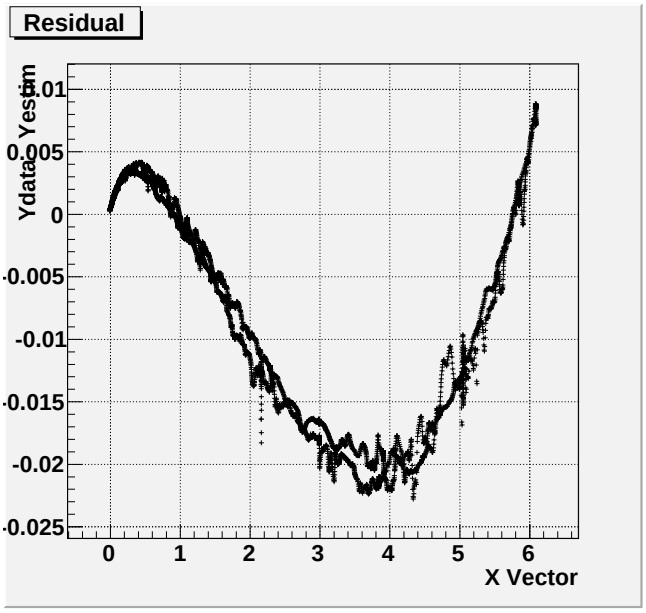

Figure 116: Residual plot #1 of Perkin Elmer 96

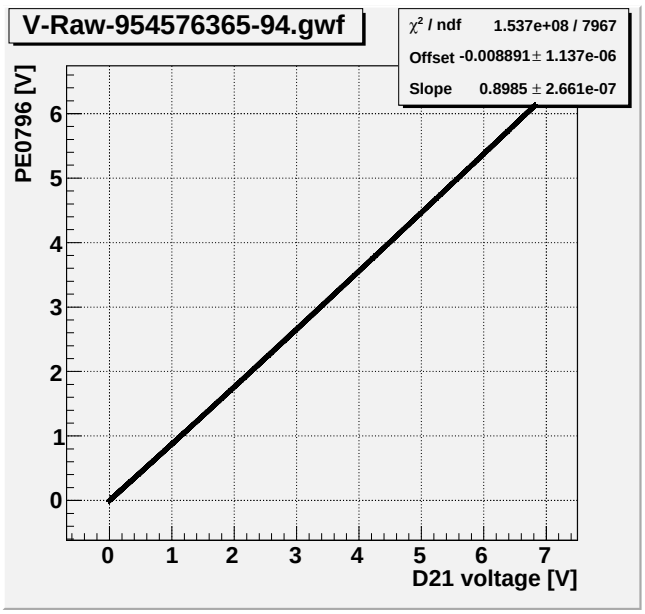

Figure 117: Linear fit #2 of Perkin Elmer 96

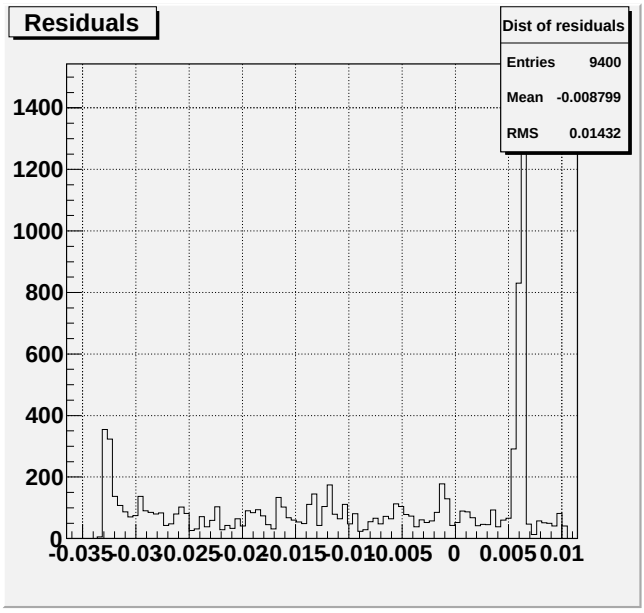

Figure 118: Residual distribution #2 of Perkin Elmer 96

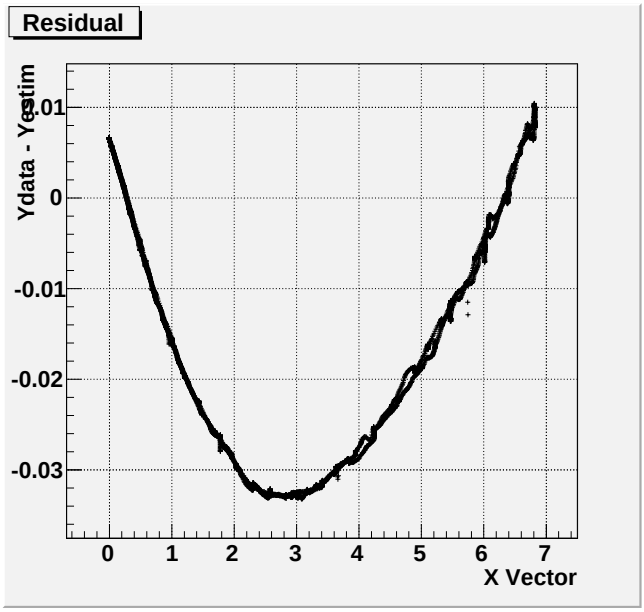

Figure 119: Residual plot #2 of Perkin Elmer 96

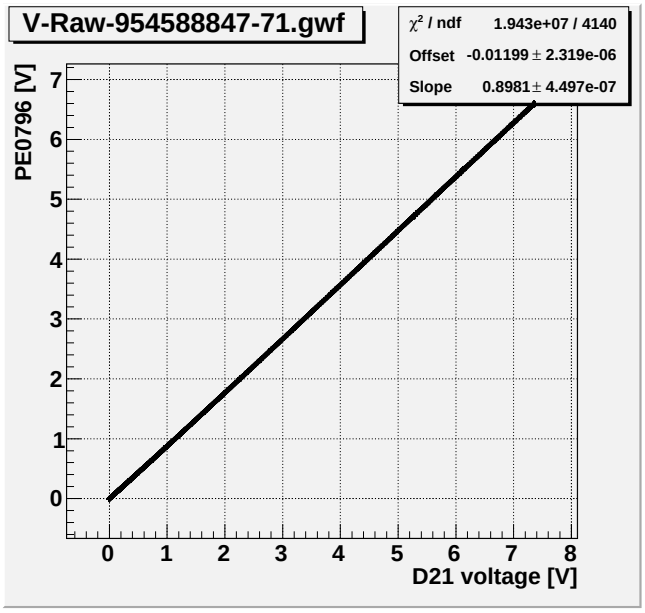

Figure 120: Linear fit #3 of Perkin Elmer 96

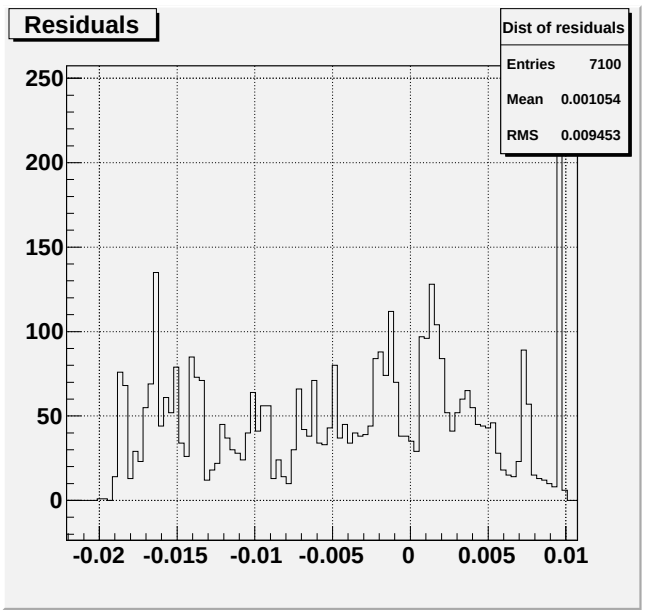

Figure 121: Residual distribution #3 of Perkin Elmer 96

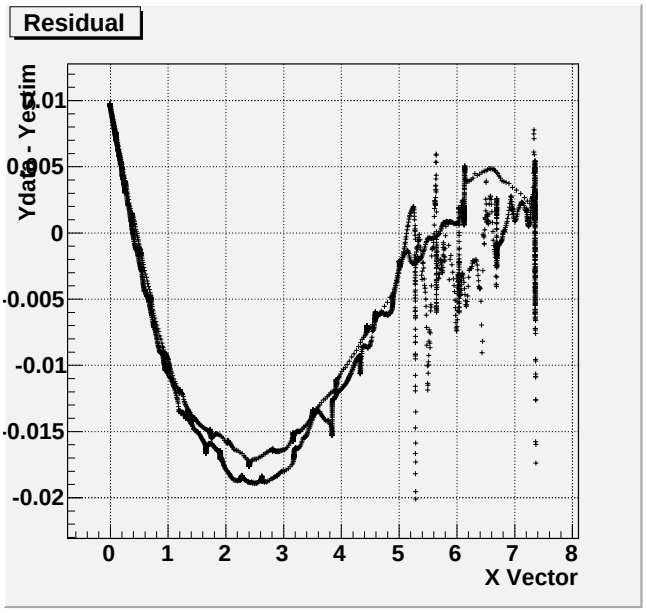

Figure 122: Residual plot #3 of Perkin Elmer 96

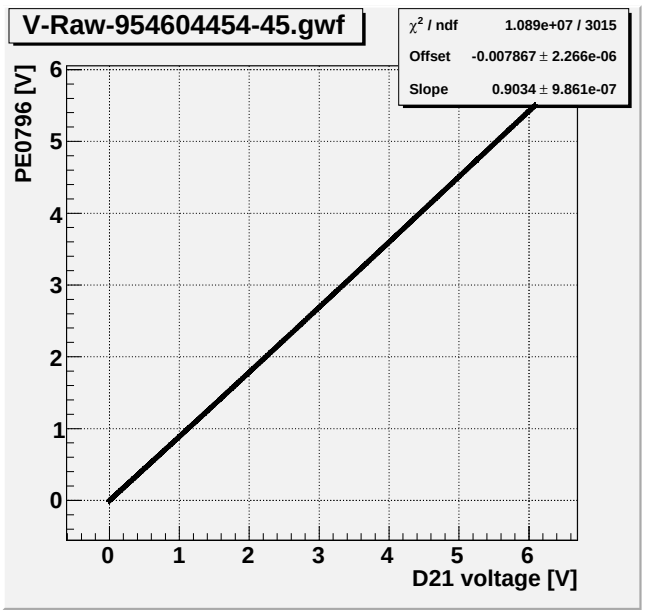

Figure 123: Linear fit #4 of Perkin Elmer 96

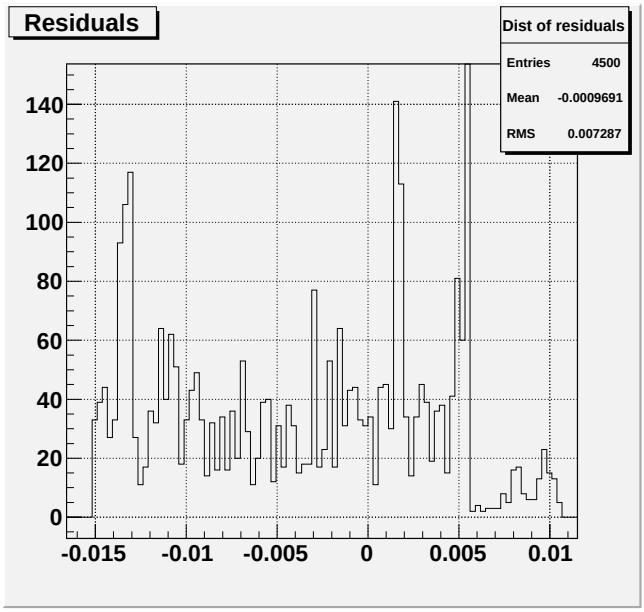

Figure 124: Residual distribution #4 of Perkin Elmer 96

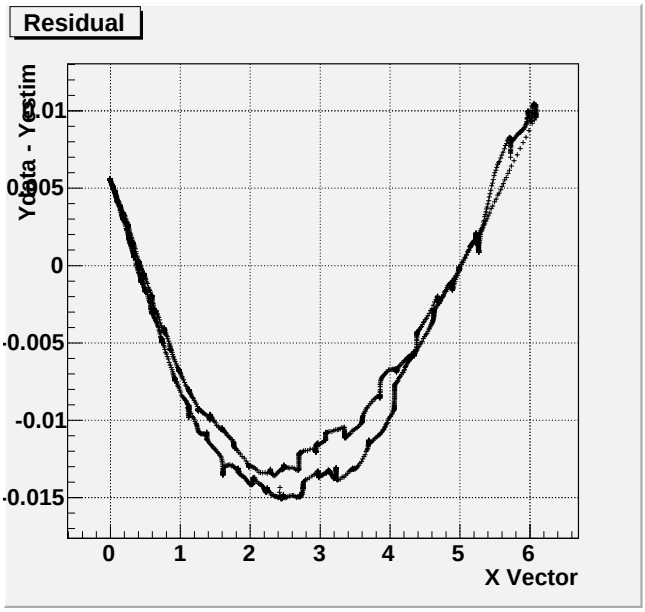

Figure 125: Residual plot #4 of Perkin Elmer 96

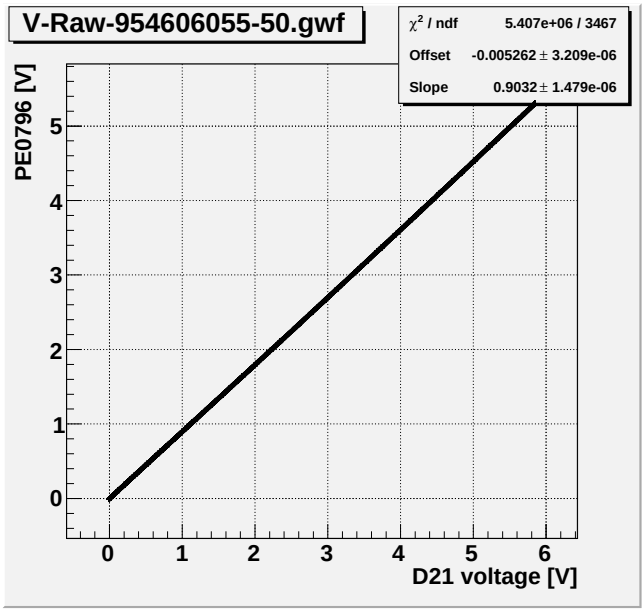

Figure 126: Linear fit #5 of Perkin Elmer 96

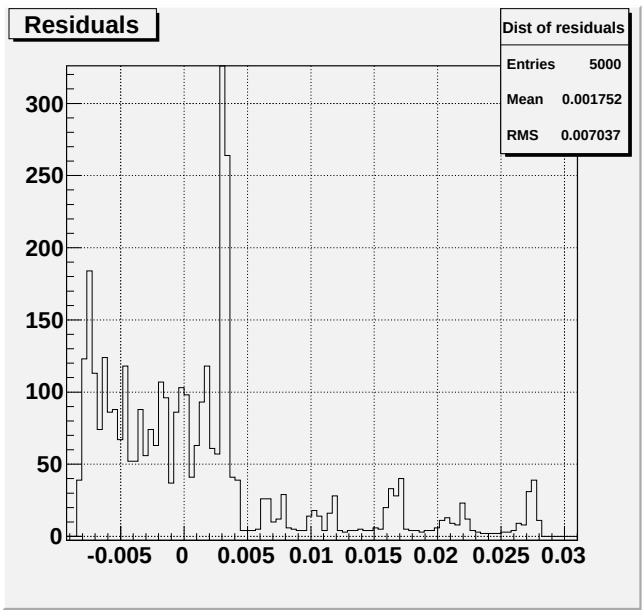

Figure 127: Residual distribution #5 of Perkin Elmer 96

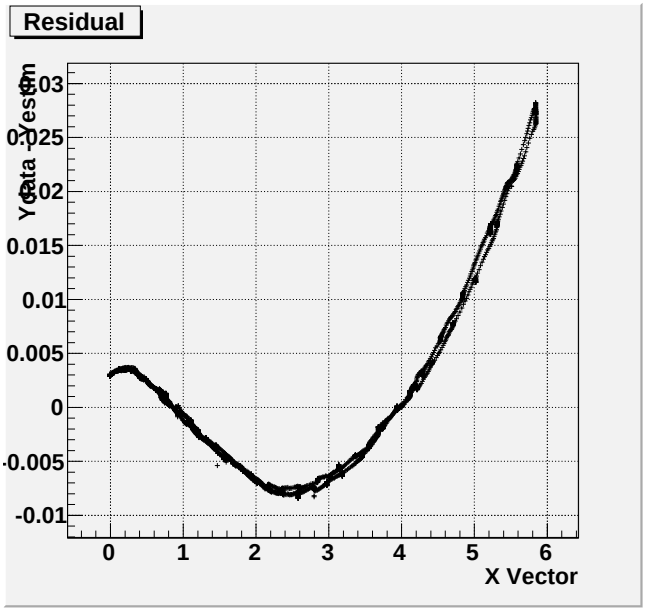

Figure 128: Residual plot #5 of Perkin Elmer 96

I Perkin Elmer 97

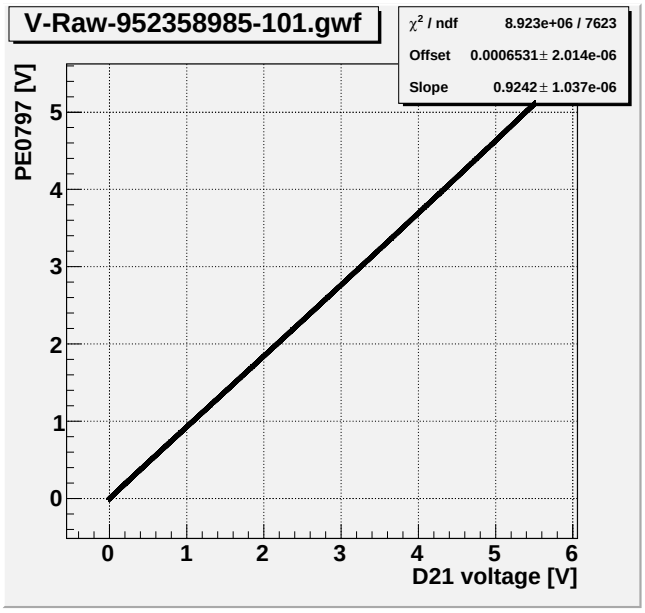

Figure 129: Linear fit #1 of Perkin Elmer 97

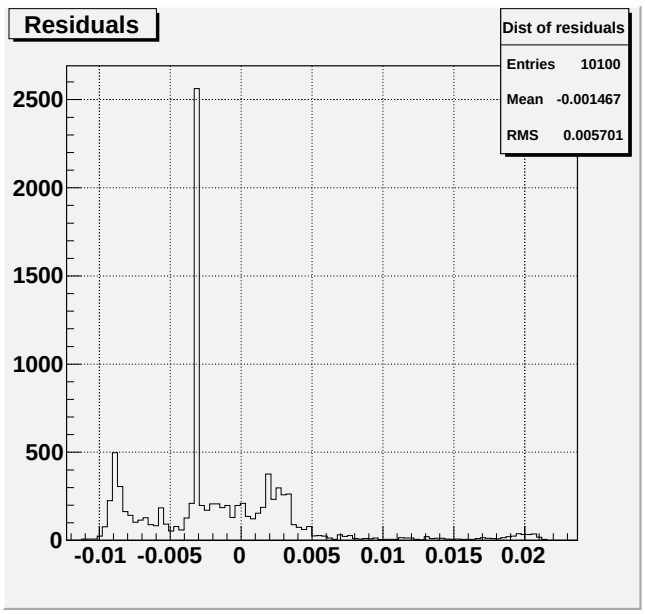

Figure 130: Residual distribution #1 of Perkin Elmer 97

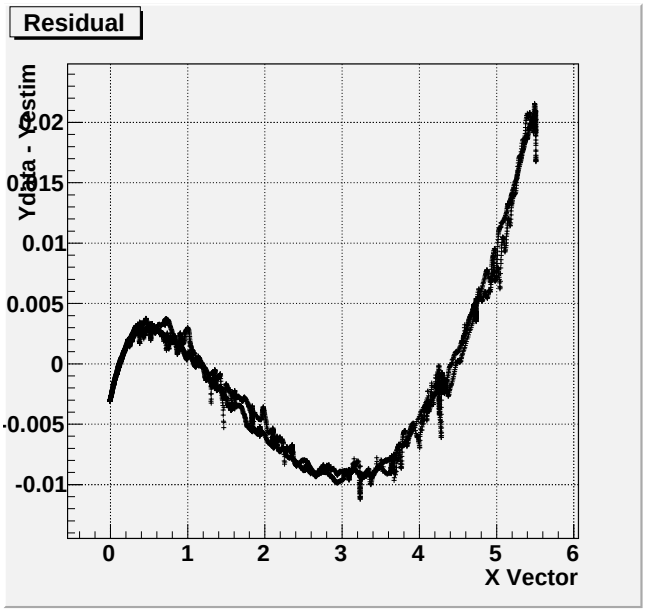

Figure 131: Residual plot #1 of Perkin Elmer 97

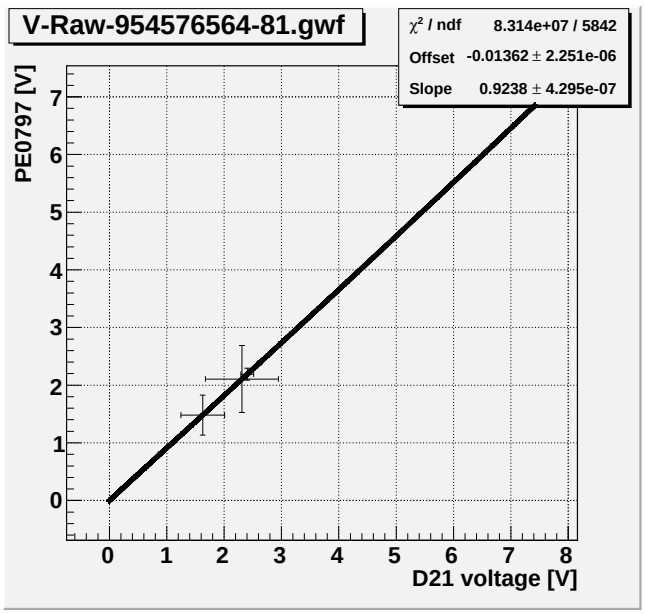

Figure 132: Linear fit #2 of Perkin Elmer 97

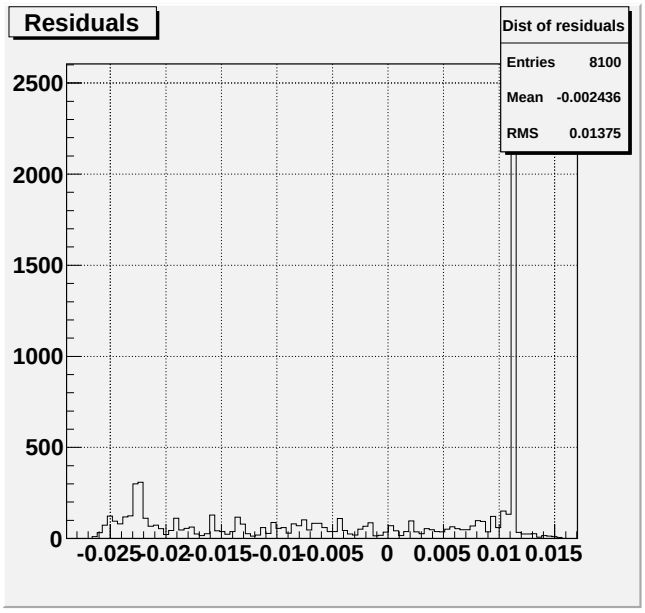

Figure 133: Residual distribution #2 of Perkin Elmer 97

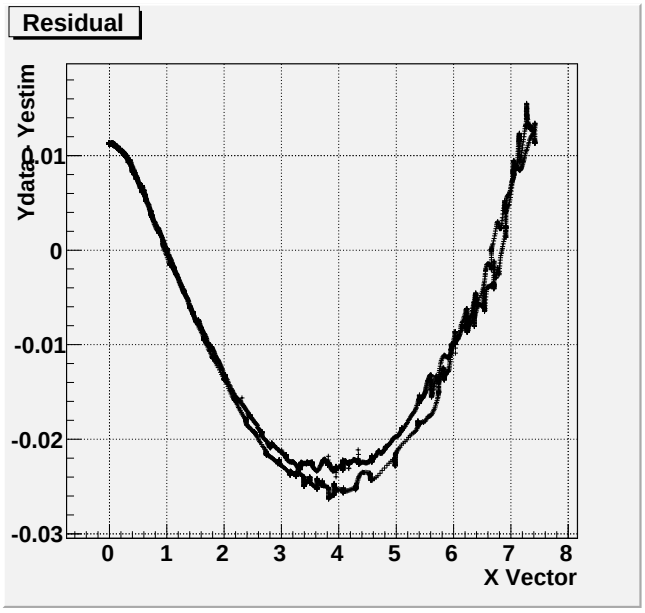

Figure 134: Residual plot #2 of Perkin Elmer 97

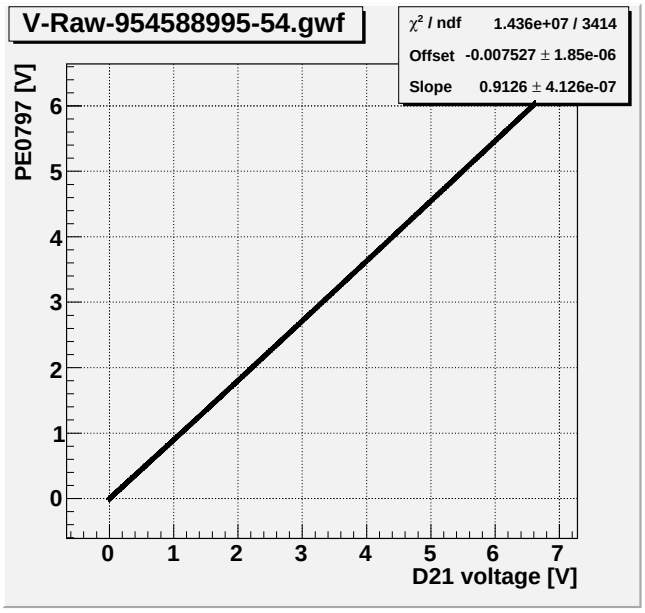

Figure 135: Linear fit #3 of Perkin Elmer 97

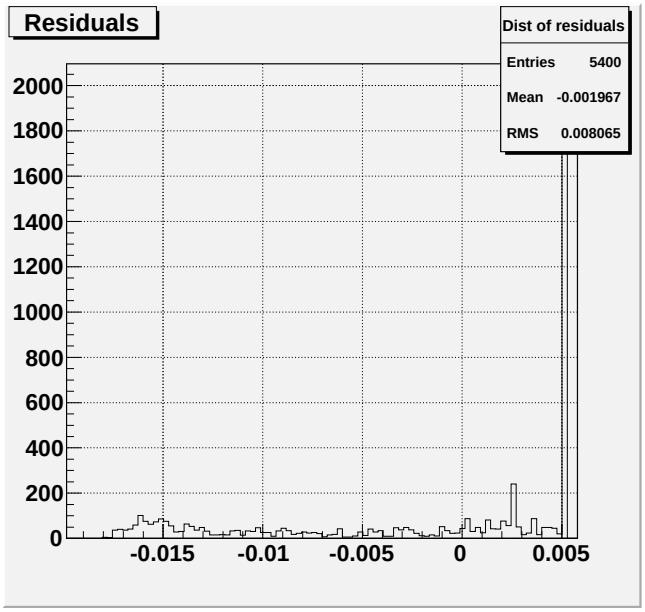

Figure 136: Residual distribution #3 of Perkin Elmer 97

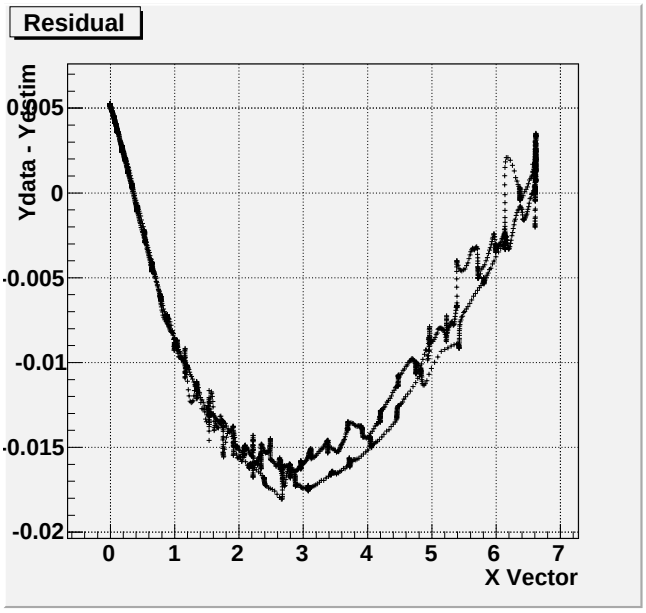

Figure 137: Residual plot #3 of Perkin Elmer 97

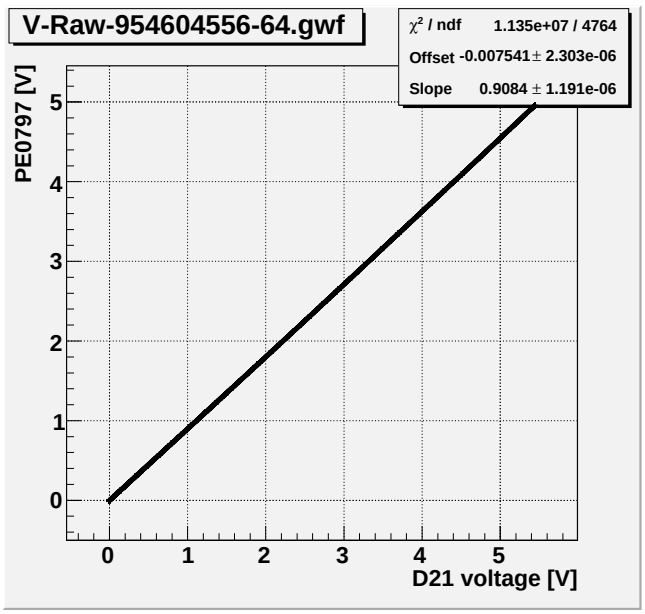

Figure 138: Linear fit #4 of Perkin Elmer 97

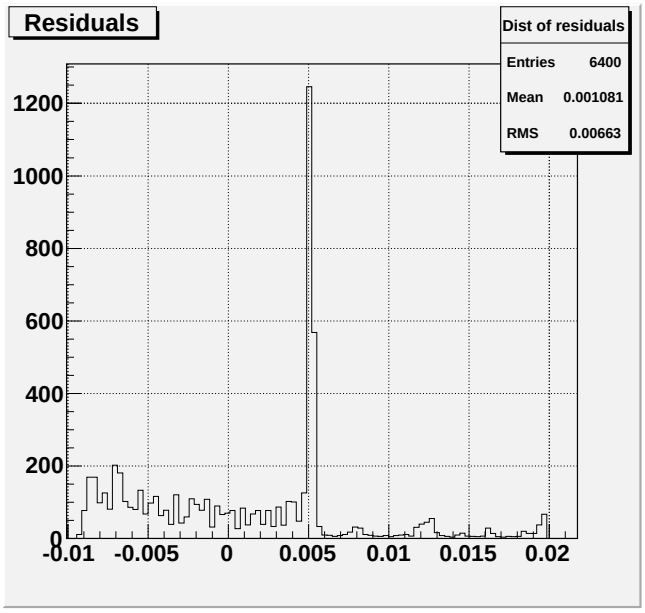

Figure 139: Residual distribution #4 of Perkin Elmer 97

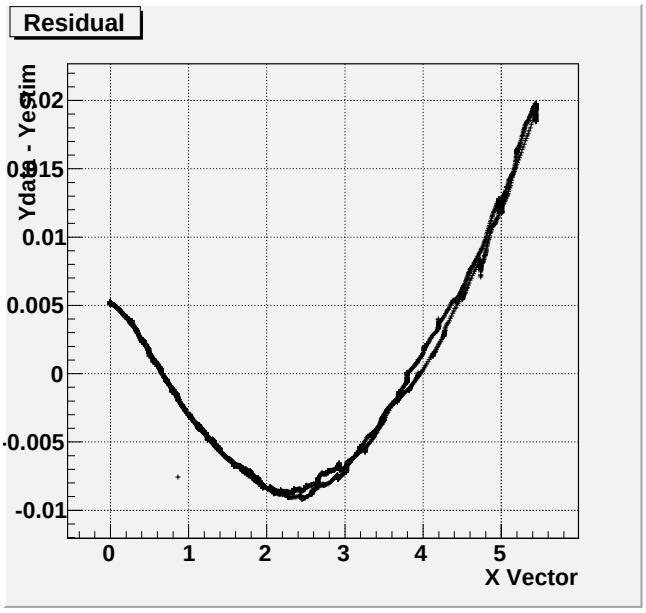

Figure 140: Residual plot #4 of Perkin Elmer 97

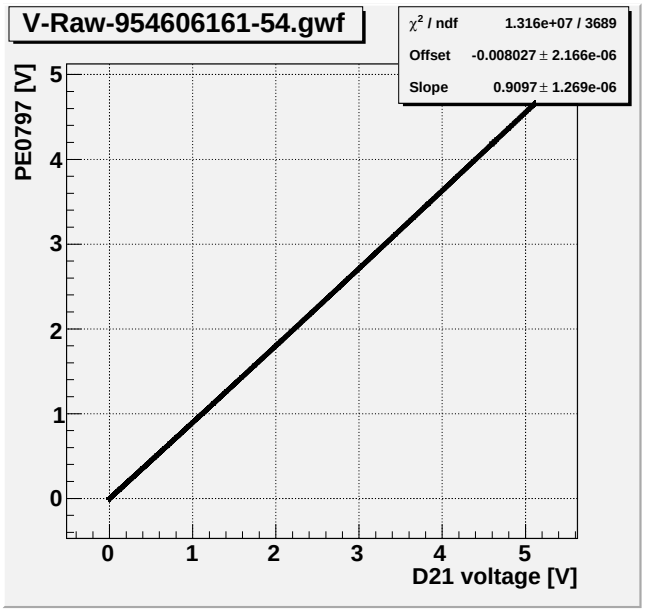

Figure 141: Linear fit #5 of Perkin Elmer 97

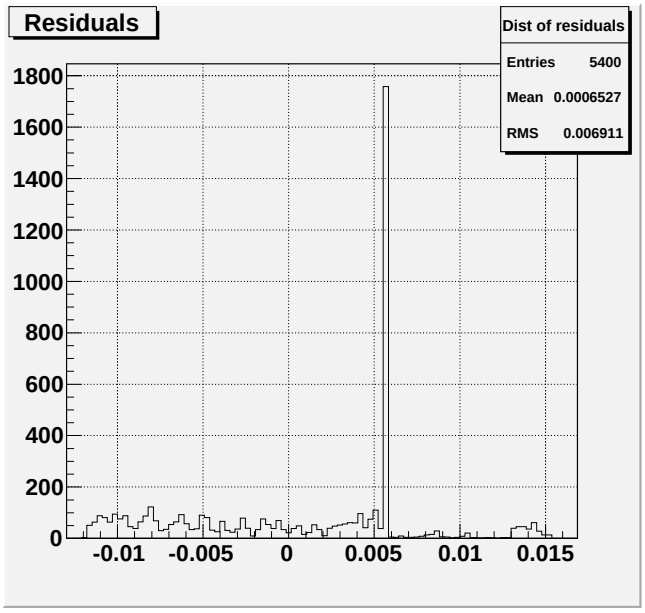

Figure 142: Residual distribution #5 of Perkin Elmer 97

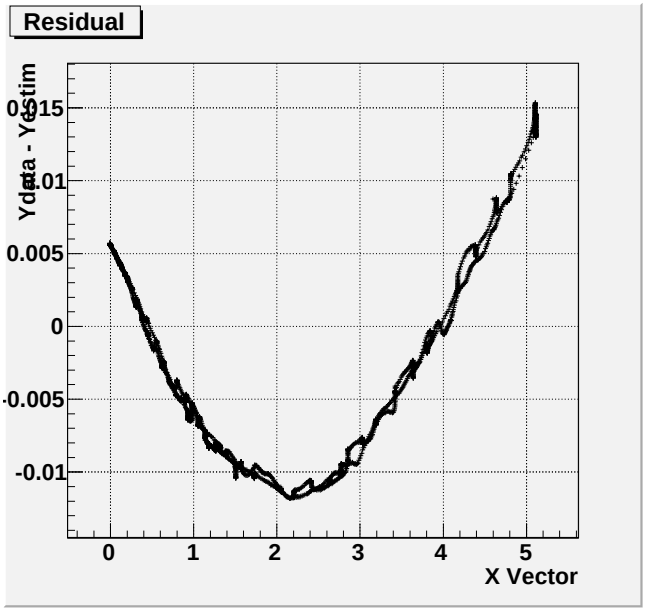

Figure 143: Residual plot #5 of Perkin Elmer 97

J Perkin Elmer 98

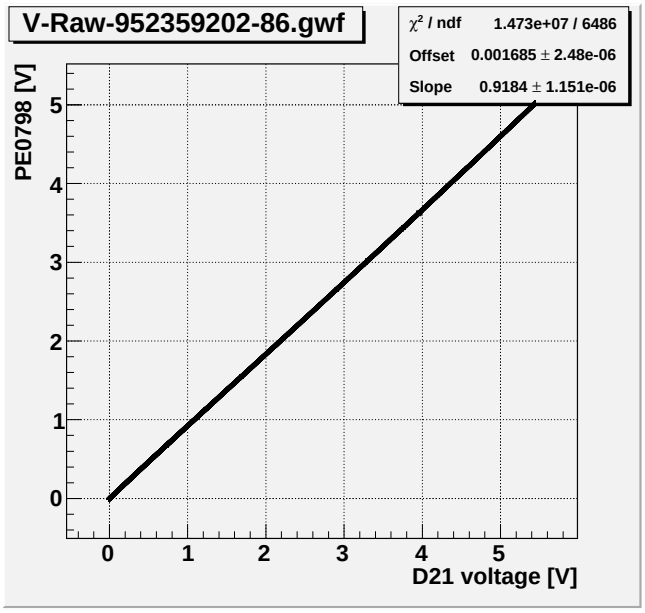

Figure 144: Linear fit #1 of Perkin Elmer 98

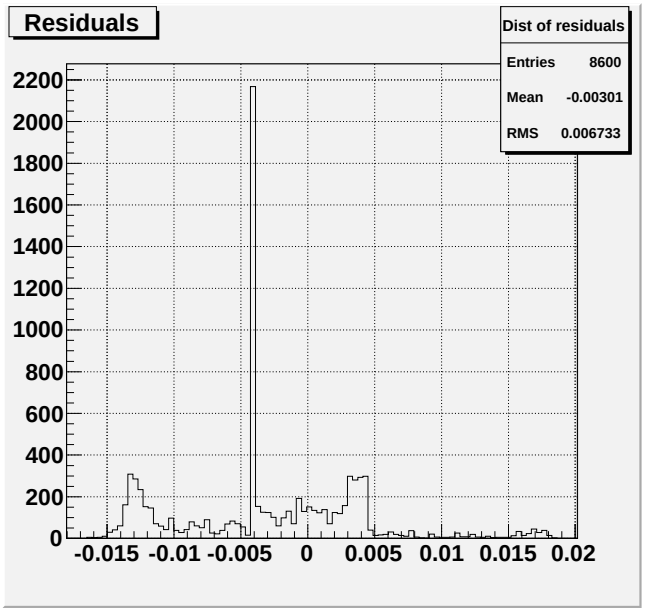

Figure 145: Residual distribution #1 of Perkin Elmer 98

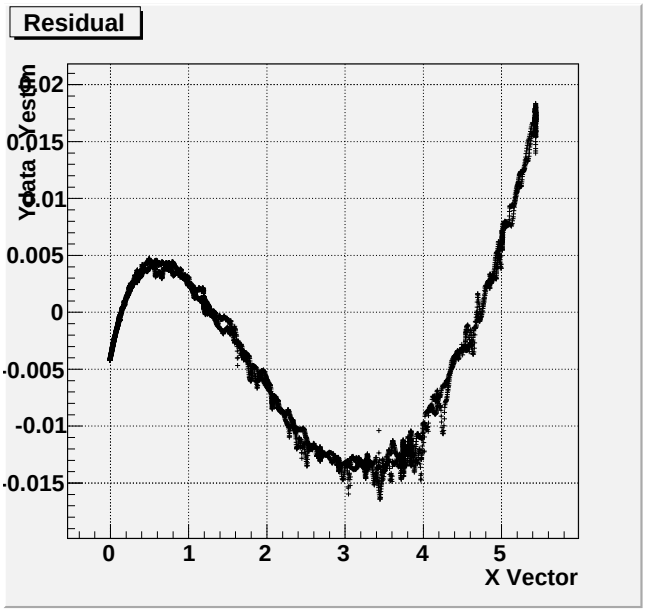

Figure 146: Residual plot #1 of Perkin Elmer 98

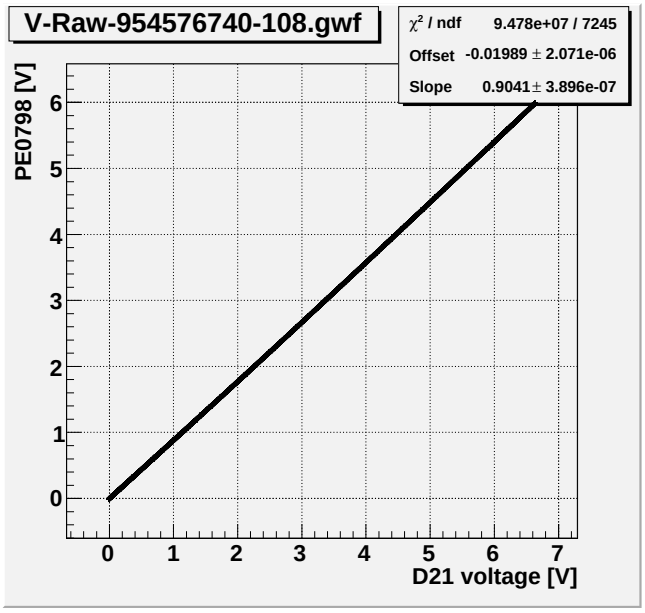

Figure 147: Linear fit #2 of Perkin Elmer 98

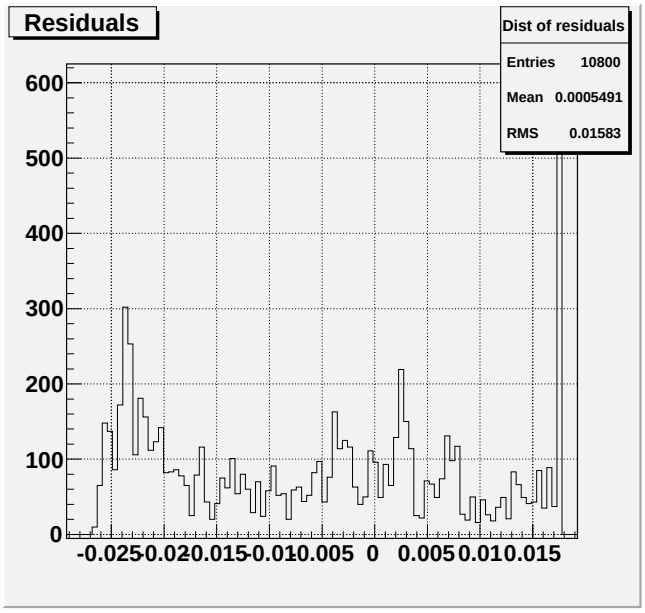

Figure 148: Residual distribution #2 of Perkin Elmer 98

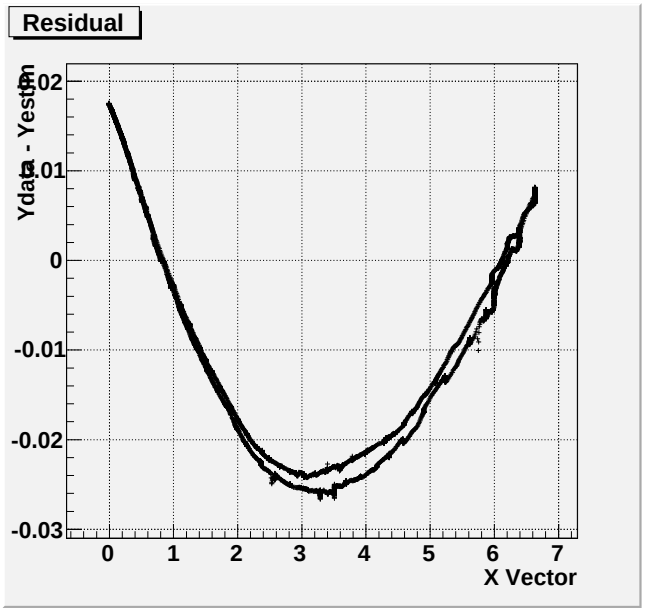

Figure 149: Residual plot #2 of Perkin Elmer 98

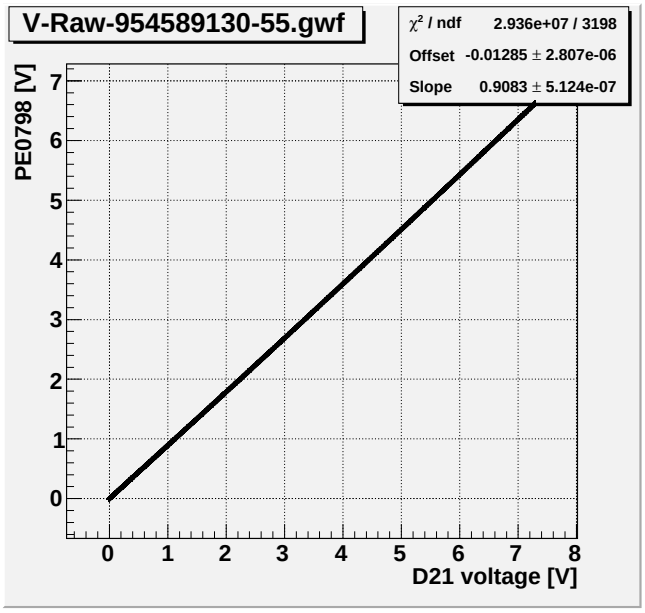

Figure 150: Linear fit #3 of Perkin Elmer 98

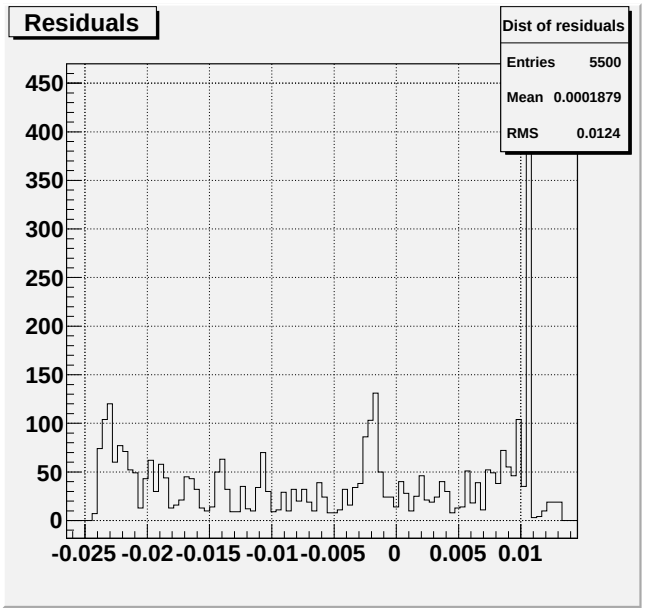

Figure 151: Residual distribution #3 of Perkin Elmer 98

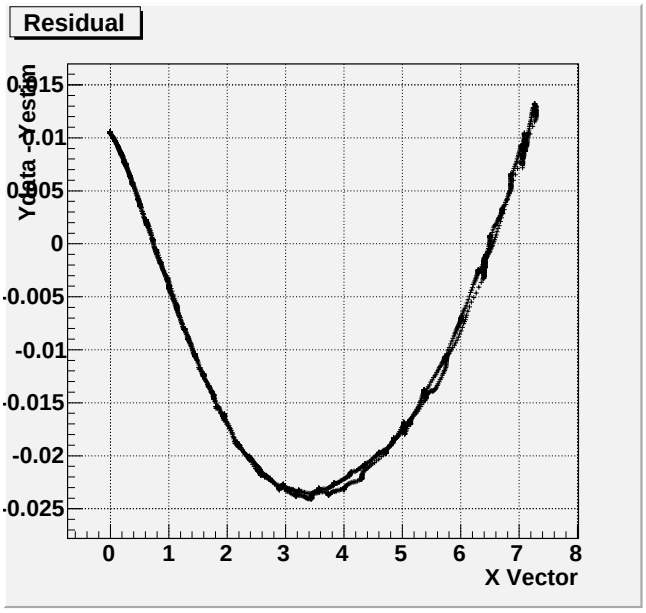

Figure 152: Residual plot #3 of Perkin Elmer 98

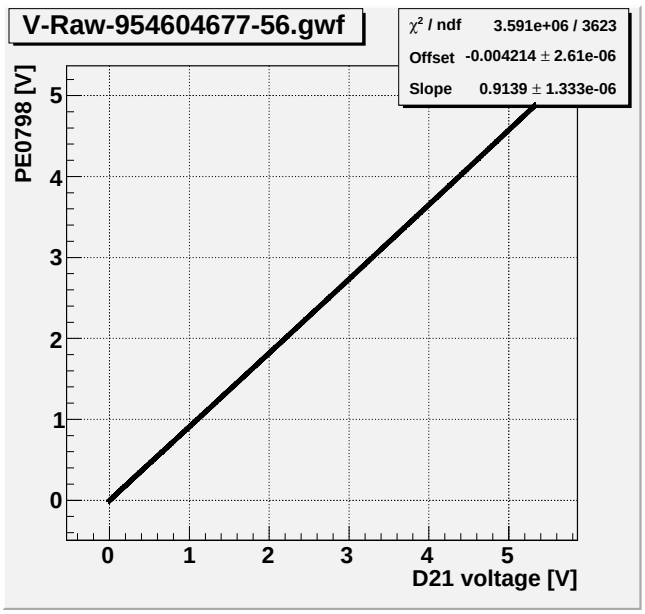

Figure 153: Linear fit #4 of Perkin Elmer 98

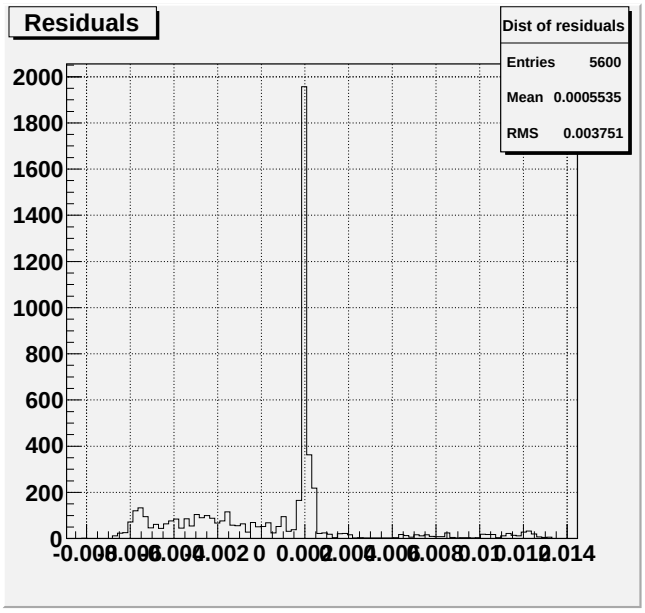

Figure 154: Residual distribution #4 of Perkin Elmer 98

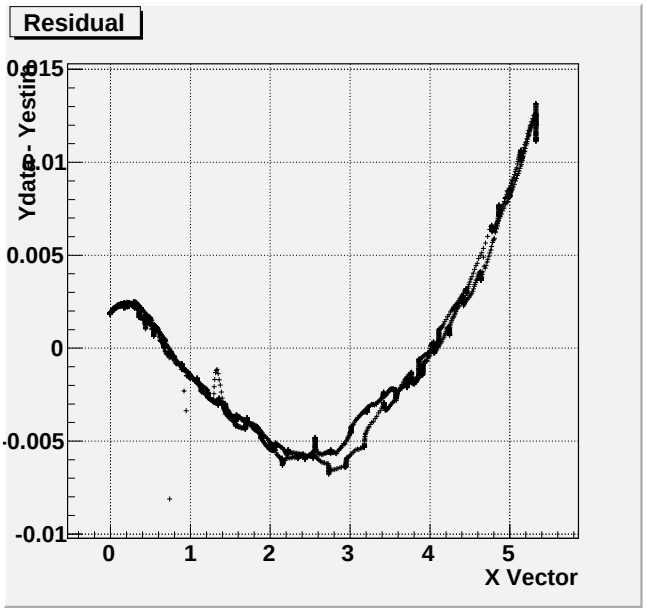

Figure 155: Residual plot #4 of Perkin Elmer 98

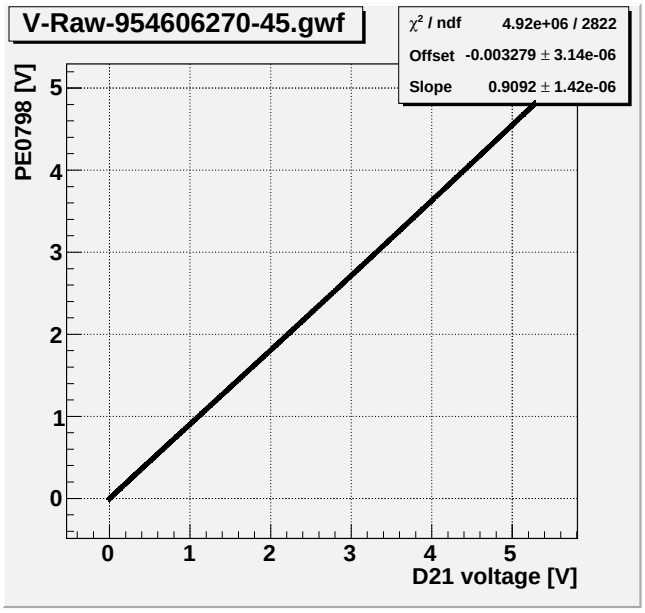

Figure 156: Linear fit #5 of Perkin Elmer 98

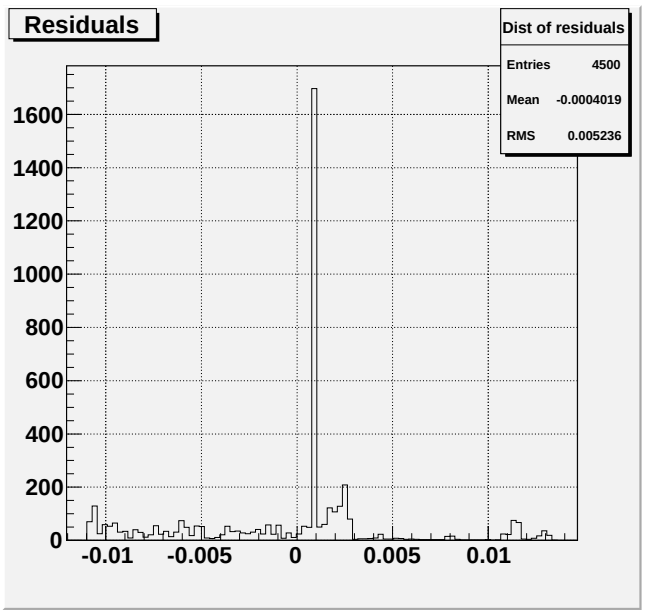

Figure 157: Residual distribution #5 of Perkin Elmer 98

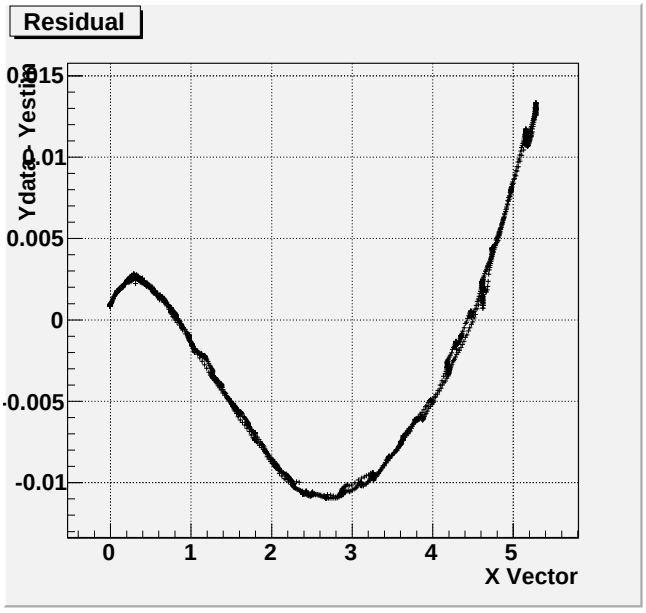

Figure 158: Residual plot #5 of Perkin Elmer 98